NACA TN 2980

NATIONAL ADVISORY COMMITTEE FOR AERONAUTICS

TECHNICAL NOTE 2980

THE AERODYNAMIC CHARACTERISTICS OF AN ASPECT-RATIO-20 WING HAVING THICK AIRFOIL SECTIONS AND EMPLOYING BOUNDARY-LAYER CONTROL BY SUCTION

By Bennie W. Cocke, Jr., Marvin P. Fink,
and Stanley M. Gottlieb

Langley Aeronautical Laboratory
Langley Field, Va.

Washington
August 1953

NATIONAL ADVISORY COMMITTEE FOR AERONAUTICS

TECHNICAL NOTE 2980

THE AERODYNAMIC CHARACTERISTICS OF AN ASPECT-RATIO-20 WING HAVING THICK AIRFOIL SECTIONS AND EMPLOYING BOUNDARY-LAYER CONTROL BY SUCTION

By Bennie W. Cocke, Jr., Marvin P. Fink,
and Stanley M. Gottlieb

SUMMARY

An investigation has been conducted to study the aerodynamic characteristics of an aspect-ratio-20 wing having thick airfoil sections and employing boundary-layer control by suction. Data from model tests in both the Langley full-scale tunnel and the Langley low-turbulence pressure tunnels are included. The results indicate the effects of varying suction flow rate, suction-slot configuration, wing surface condition, flap deflection, and Mach number.

The results indicate that, through the use of boundary-layer control by suction, trailing-edge separation was controlled and lift-drag ratios as high as 30.8 were attained in the lift-coefficient range from 0.9 to 1.0 for the smooth-wing configuration. Up to a Mach number of 0.44, test results show compressibility effects to be only minor for the lift-coefficient range up to and including 1.0. With full-span trailing-edge flaps installed and maximum suction flow rates applied, maximum lift coefficients of 2.5 and 4.2 were obtained for flaps-neutral and flaps-deflected conditions, respectively.

INTRODUCTION

The use of high-aspect-ratio wings as a means for reducing the induced drag and thus increasing the maximum lift-drag ratio has been common practice for many years. Structural considerations indicate, however, that increases in the root-section thickness ratio must accompany increases in the aspect ratio. For airfoil-section thickness ratios above a certain value, the profile drag increases rapidly with increasing airfoil thickness ratio because of boundary-layer separation in the vicinity of the trailing edge. As a consequence, increases in the aspect ratio above a certain value cause increases in the profile drag which are greater than the decreases in induced drag. Thus, there is a limiting

aspect ratio above which no improvements in lift-drag ratio are obtained. For conventional straight wings designed on the basis of a ratio of root thickness to span of 1/35, this limiting aspect ratio is about 12.

A two-dimensional investigation of airfoil sections as thick as 40 percent has indicated that trailing-edge separation can be eliminated by boundary-layer control (ref. 1). An analysis of several finite wings having high aspect ratios and thick root sections with boundary-layer control was also presented in reference 1. This analysis, which was based on wings having a ratio of root thickness to span of 1/35 and a rough leading-edge condition, indicated the possibility that the use of thick root sections and aspect ratios of the order of 20 would yield lift-drag ratios higher than those obtainable with conventional straight wings without boundary-layer control. The investigation reported herein was made to determine experimentally the aerodynamic characteristics of a high-aspect-ratio, three-dimensional wing, designed along the lines indicated by the analysis of reference 1.

The three-dimensional wing was designed with an aspect ratio of 20, a taper ratio of 0.286, and -5° 20' of twist (washout), and with provisions for a full-span suction slot located at the 60-percent chord point on the upper wing surface. The airfoil sections varied from an NACA 64,2-437 profile at the root to an NACA 64_5-424 profile at the tip. Two semispan models were constructed with semispans of 22.5 feet and 2.695 feet. These models were tested in the Langley full-scale tunnel and Langley low-turbulence pressure tunnel, respectively.

This report presents the results of these two investigations which included studies of the effects of varying suction flow rate, suction-slot configuration, flap deflection, wing surface condition, and Mach number on the aerodynamic characteristics of the wing.

SYMBOLS

C_L wing lift coefficient, L/qS

C_D wing total drag coefficient, $\frac{D}{qS} + C_{D_b}$

C_m pitching-moment coefficient about quarter-chord point, Pitching moment/$qS\bar{c}$

C_{D_o} wing profile-drag coefficient, $\frac{2}{S}\int_0^{b/2} c_{d_o} c \, dy$

c_{d_o}	section profile-drag coefficient
C_{D_b}	blower-power drag coefficient, $C_P C_Q \frac{S'}{S}$
C_P	total-pressure-loss coefficient, $\frac{H_o - H_d}{q_o}$
C_Q	flow coefficient, $Q/V_o S'$
c	local airfoil chord, ft
$\bar{c}$	mean aerodynamic chord, ft
q	free-stream dynamic pressure, lb/sq ft
ρ	mass density, slugs/cu ft
R	free-stream Reynolds number based on mean aerodynamic chord
b/2	wing semispan, ft
S	wing area, sq ft
S'	wing area affected by suction, sq ft
L	wing lift, lb
D	wing drag, lb
L/D	wing lift-drag ratio
α	angle of attack, deg
δ_f	flap deflection, deg
M	Mach number, V_o/a
M_{cr}	critical Mach number
V_o	free-stream velocity, ft/sec
a	free-stream speed of sound, ft/sec
Q	quantity of air removed through suction slot, cu ft/sec

H_o free-stream total pressure, lb/sq ft

H_d duct total pressure (measured at wing root), lb/sq ft

y distance along span from wing root, ft

APPARATUS AND TESTS

Models

The models used in the two investigations were identical in external geometry and had an aspect ratio of 20 and a taper ratio of 0.286. Both models were designed to have -5° 20' geometric twist (washout); however, because of construction difficulties the 2.695-foot span model had a twist of -4° 49'. The wings tapered in thickness along straight-line elements from an NACA 64,2-437 section at the root to an NACA 64$_5$-424 section at the 52-percent-semispan station with constant section from the 52-percent-semispan station to the tip. The basic design parameters for the models were determined from consideration of several factors. An aspect ratio of 20 and a taper ratio of 0.2 were indicated on the basis of reference 1. Analysis by the methods of reference 2 indicated poor stalling characteristics for an untwisted wing having a taper ratio of 0.2. A compromise was therefore indicated and a wing having a geometric twist of -5° 20' and a taper ratio of 0.286 was chosen. Wing-root thickness was based on an assumed structural-design consideration of having the span-to-root thickness ratio equal to 35. Both models had provision for full-span suction slots located on the upper surface of the wing at the 60-percent-chord station. Suction was applied to the semispan models by externally located blowers connected to the wing ducts at the wing root. Mechanical tares due to ducting were eliminated through the use of a mercury seal where the blower ducting attached to the wing ducting; the effects of suction forces across the seal on lift and drag were eliminated by alining the ducting at the seal so that all reaction was in the side-force plane. The internal ducting on each model was carefully designed to minimize blower-power losses. The wing ducts were not restricted by wing structure at any point. The suction slots of both models had ramp angles of 45°, rounded slot entry lips, and small internal diffuser angles. For the small model a full-span slot having a width of 1 percent of the local chord was used in all tests. The large model was tested with three different slot arrangements, namely, (1) a slot tapering from 2 percent chord at the root to 0 percent chord at the $0.52\frac{b}{2}$ station, (2) a 1.5-percent-chord slot extending from the root to the $0.52\frac{b}{2}$ station, and (3) a full-span constant-1.5-percent-chord slot. The general arrangement and principal dimensions of the basic models are shown in figure 1 and the airfoil ordinates are given in table I.

The 22.5-foot semispan model tested in the Langley full-scale tunnel was equipped with a full-span 30-percent-chord Fowler-type flap which could be replaced by a smooth trailing-edge block for basic wing tests. Ordinates for the flap, as well as hinge-point locations, are presented in table II. Sketches of the flap arrangement are presented in figure 2.

In order to avoid repetition in the following discussion, the 22.5-foot semispan wing is referred to as model I and the 2.695-foot semispan wing, as model II.

Tests

Model I.- Model I was mounted for tests on the reflection plane in the Langley full-scale wind tunnel as shown in figure 3(a). Tests were made with the boundary-layer suction slot sealed and faired, as well as with the three different suction-slot configurations previously described. For all configurations, the suction slot was located at the 60-percent-chord station on the upper surface of the wing. Each model configuration was tested with the full-span trailing-edge flaps retracted and deflected and with suction flow coefficients ranging from 0 to 0.035.

Lift-, drag-, pitching-moment-, and duct-pressure-loss-coefficient data were obtained over the angle-of-attack range from the angle for zero lift through the angle of stall for each suction flow coefficient investigated. Total and static pressures for use in determining blower power required were measured in the internal ducts at the wing root for each condition by means of rakes of total- and static-pressure tubes. Profile-drag measurements were also obtained by wake surveys at 26 spanwise stations for two of the suction-slot configurations at angles of attack covering the lift-coefficient range from $C_L = 0$ to $C_L = 1.0$. Flow separation on the wing surface and at the wing-reflection-plane juncture was studied by means of small wool tufts attached to the wing surface.

The wing surface condition for most of the test program was maintained smooth. This condition could best be described by stating that the wing skin was 1/4-inch plate rolled to contour, sanded and filled smooth to the touch, spray painted and lightly sanded. A limited number of tests were made for the full-span suction configuration with leading-edge roughness applied. This condition was obtained by spreading No. 60 (0.011-inch diameter) carborundum grains across the complete-span 0.08-chord surface distance back from the leading edge on both the upper and lower surface, the carborundum covering approximately 5 to 10 percent of the area over which the particles were spread. The Reynolds number range for these tests was limited to 1.5×10^6 to 2.25×10^6, which corresponds to a Mach number range from approximately 0.09 to 0.11.

Model II.- Model II was mounted on an electrical-resistance strain-gage balance and the ceiling of the test section of the low-turbulence pressure

tunnel was used as a reflection plane. Leakage through the tunnel wall, where the model passed through to the balance system, was minimized by a flush-type labyrinth seal attached to the model at the wall as shown in figure 1.

The prime objective in testing this model was to determine the effects of Mach number on the characteristics of a wing of this type for a range of lift coefficients corresponding to the cruise condition. Tests were therefore made for only one model configuration (full-span, 1-percent slot, plain wing) with the range of suction flow coefficients limited to those of interest for cruising flight (C_Q = 0.002 to 0.010). The suction slot on this model was divided into three spanwise sections, each connected to an individual duct (fig. 3(b)); thus, a means of varying suction flow rates between stations across the wing span was provided. Preliminary tuft investigations, however, indicated a localized region of separation occurring at the juncture of the inboard and center slot sections when the slot sections were operating at different flow rates. All subsequent tests were therefore made with a constant flow coefficient across the span.

Lift-, drag-, pitching-moment-, and pressure-loss-coefficient data were measured for each flow condition over the angle-of-attack range from $\alpha = 0^\circ$ through the angle of attack for stall at a Mach number of 0.2. For the more promising flow conditions, data were obtained up to a Mach number of 0.44. The Reynolds number range of these tests, based on the mean aerodynamic chord of the model, varied from 0.71×10^6 to 2.31×10^6 and the Mach number ranged from 0.12 to 0.44.

For model configurations with roughness, strips of 0.004-inch-diameter carborundum particles were embedded in a thin coat of shellac located at the 10-percent-chord point on the upper and lower wing surfaces. The strips were 1/4 inch wide at the wing root and tapered to 1/8 inch at the tip.

METHODS AND CORRECTIONS

Data for both models have been corrected for tunnel-wall effects and all force-test drag data have been corrected to include the drag equivalent of the blower power required for each suction condition. The expression used for computing blower drag $C_P C_Q \frac{S'}{S}$ has been shown to be valid (ref. 3) if the efficiency of the blower system is the same as the efficiency of the propulsive system.

Data for model I have been corrected for tunnel stream-angle misalinement; whereas data from model II have not been corrected. Inasmuch as the

primary test objective (model II) was a check of Mach number effects on a wing of this type, an exact stream-angle evaluation did not appear to be justified.

Basic data presented for each of the semispan models have not been corrected for the effects of tunnel-wall boundary layers which, expressed in terms of model semispans, had thicknesses of 1.5 percent of the semispan for model I and 3 percent of the semispan for model II. Tuft studies made for model I did not indicate any extensive separation at the wing-root juncture; therefore, root-interference evaluation did not appear to be justified for all the test conditions. Wake surveys by the momentum method were made, however, for the more optimum test conditions and drag values used in final lift-drag-ratio calculations for model I have been corrected for the values of interference drag indicated by these surveys.

PRESENTATION OF DATA

Lift-, drag-, pitching-moment-, and suction-pressure-loss-coefficient data for model I are presented in figures 4 to 15. Data are shown for the wing with suction slot sealed and faired (fig. 4), for the wing with suction applied to the inboard 0.52 semispan (figs. 5 to 7), and for the wing with suction applied full span (figs. 8 to 15). These data include the effects of suction-flow variation, flap deflection, and model surface condition (leading-edge roughness). Profile-drag measurements obtained for model I by the wake-survey method (ref. 4) for several conditions are shown in figures 16 and 17 and are compared in figure 18 with profile-drag values computed from force-test results by the method of reference 2. Figures 19 and 20 show the relation of blower drag, profile drag, and total drag of the wing for a range of suction-flow conditions at two lift coefficients. Maximum-lift data for the range of test variables are summarized in figure 21 and the variations of lift-drag ratio with lift coefficient for the more pertinent test conditions are shown in figures 22 to 24.

Representative data obtained from tests of model II are presented in figures 25 to 28. These data are presented primarily to indicate effects of Mach number for a wing of this type with and without leading-edge roughness. Correlation of these data with data from model I is not intended because of the previously discussed differences in model and test conditions. Summary plots of the effects of Mach number on lift-drag ratio for model II are presented in figure 29. Predicted critical Mach numbers for the root section of the wing calculated by the method of reference 5 from low-speed pressure measurements obtained from model I are presented in figure 30 for a lift-coefficient range from -0.2 to 1.4.

RESULTS AND DISCUSSION

Drag Characteristics

The rapid increase in drag above a lift coefficient of 0.6 shown by the data in figure 4 for the basic wing (slot sealed) clearly indicates the effects of extensive trailing-edge separation on the thick root sections. Tuft studies made in conjunction with force tests indicated that some degree of trailing-edge separation existed at all angles of attack over the root sections of the wing with the result that the minimum wing drag measured at a lift coefficient of 0 was 0.017. With suction applied to the wing through either the semispan or full-span suction slots, the rapid increase in profile drag associated with extensive trailing-edge separation could be postponed to higher and higher lift coefficients by increasing suction flow rates as evidenced in figures 5 to 15. From these results, however, it is obvious that, for all except the lower flow-coefficient range, the wing drag (including blower-power drag) becomes excessive despite the elimination of trailing-edge separation because of the rapid increase in blower-power requirements with increasing flow coefficient.

Effect of suction flow rate.- The relation of wing total drag to suction flow rate is illustrated in figures 19 and 20 by the breakdown of wing total drag into its various components for a range of suction flow coefficients for lift coefficients of 1.0 and 0.5. From these results it is apparent that, for this wing, flow rates for minimum total drag do not correspond to flow rates for minimum profile drag because of the rapid increase in blower power with increasing flow. It is also noteworthy that the 0.52 b/2 tapered-slot configuration which gave minimum total drags actually had higher profile drag throughout all but the low flow-coefficient range. The net drag reduction possible through suction, therefore, depends not only on efficient slot and duct designs but also upon maintenance of the proper relation of blower power and profile drag.

Effect of slot configuration.- In order to illustrate the effect of slot design consider the flow characteristics of the full-span constant-percent-chord and 0.52 b/2 tapered-slot arrangements investigated. For the full-span 1.5-percent-chord slot, local flow coefficients at all spanwise stations will be very nearly constant (provided sufficiently large duct-to-slot area ratio is maintained (ref. 6)). With the tapered slot on the inboard 0.52 b/2 only, however, local suction flow rates will vary across the span for any wing suction coefficient $\left(C_Q = \frac{Q}{V_o S'}\right)$ in such a way that the greatest local suction flow ratio will be obtained for the thick root sections and will diminish outboard to 0 where the wing becomes 24 percent thick.

Close study of two-dimensional section data (ref. 1) indicates that, in order to minimize the blower-power requirement, local suction flow rates should vary across the span. For example, consider the wing at a lift coefficient of approximately 1.0. Section data indicate that, for the thick root sections (thickness ratio, 0.37), a flow coefficient of approximately 0.01 would be near optimum whereas, for the outboard sections (thickness ratio, 0.24), this flow rate would represent a waste of blower power because the greatest drag reduction for this section is obtained at much lower flow coefficients. On the basis of these data, therefore, the full-span, constant-1.5-percent-chord slot would be expected to be less efficient for drag reduction than a tapered slot designed to expend the greatest portion of the blower power for suction at the thick root sections where separation losses are the greatest. The results of the present tests (figs. 19 and 20) with the two types of slots show that the three-dimensional tests confirm the predictions in this respect and the lowest wing total drags were obtained with the tapered slot on the inboard semispan only. Profile-drag surveys (fig. 17) with the wing smooth did not indicate any extensive separation over the outboard wing panel where suction was not applied. It should be noted, perhaps, that the seven localized drag peaks shown in figure 17 represent the seven external-flap hinge brackets installed on the lower wing surface.

Effect of Mach number.- The effect of Mach number on the drag characteristics of the smooth model as obtained from the test on model II is presented in figure 25. These results indicate no compressibility effects up to the maximum test Mach number of 0.44 at lift coefficients up to 1.4, but at higher lift coefficients a rapid rise in total drag occurs at Mach numbers greater than 0.3. These results are reasonably consistent with critical-speed predictions, based on low-speed measurements of surface pressures obtained on model I at the spanwise station at which the wing is 36 percent thick and shown in figure 30. The predicted critical Mach numbers indicated by the low-speed results vary from 0.55 at a lift coefficient of 0 to 0.42 at a lift coefficient of 1.4.

Effect of leading-edge roughness.- The low Mach number test results of model I (fig. 14) show that for the full-span suction condition severe leading-edge roughness caused drag increments of the order of 0.10 to 0.15 in the lift-coefficient range between 0 and 0.2, whereas increments of the order of 0.003 to 0.005 were obtained in the higher lift-coefficient range. Tuft studies indicated that the large increments in drag obtained at the low lift coefficients were associated with flow separation from the lower surface.

Data obtained from model II at a Mach number of 0.2 (fig. 27) show approximately the same drag increment due to roughness at $C_Q = 0.006$ as that shown for model I in the moderate-lift-coefficient range (0.4 to 1.0). For the higher Mach number condition ($M = 0.40$) which results in increased adverse pressure gradient on the airfoil, the effects of

roughness were more severe and the low-suction-flow condition $C_Q = 0.0057$ did not eliminate separation (fig. 26). A slight increase in the suction flow rate to $C_Q = 0.007$, however, was sufficient to eliminate separation at the higher Mach numbers and to minimize the effects of roughness even though model blower drag was slightly increased at the higher suction flow rates.

Lift Characteristics

Tests of the basic smooth wing with suction slot sealed and faired (fig. 4) show that, as would be expected, for very thick sections a relatively low maximum lift coefficient of 1.1 was obtained with flaps neutral. The lift-curve slope for $\delta_f = 0$ was approximately 0.1 per degree up to a C_L of 0.6 but, above this lift coefficient, extensive trailing-edge separation spreading outboard from the root section caused a large reduction in lift-curve slope. Deflecting the full-span trailing-edge flaps produced approximately constant increments in lift coefficient for the angle-of-attack range in which the lift curves were linear with a maximum increment of approximately 2.0 obtained for the 45° flap deflection. The maximum lift coefficient with flaps deflected 45° reached 2.88.

Applying suction to the wing semispan did not greatly alter the lift-curve slope in the linear range but did extend the linear lift range to higher angles of attack. As shown by figure 21, the increments in maximum lift obtained by suction with the inboard $0.52\frac{b}{2}$ slot configuration were small compared with the lift increments obtained with full-span flaps or with full-span suction. Tuft studies made in conjunction with these tests indicated that the maximum lift of the wing was limited by complete stall of the outboard wing sections to which suction was not applied. With the suction slot extended full span and maximum suction applied (fig. 21), it was possible to delay trailing-edge separation to considerably higher angles of attack, and maximum lift coefficients of 4.2 and 2.5 were reached for the flaps-deflected and flaps-removed configurations, respectively. For each of these configurations maximum lift was obtained at an angle of attack of approximately 19°. It should perhaps be noted that, with suction applied, the wing stall is very abrupt.

These results show that full-span boundary-layer suction is effective in obtaining high maximum lifts, whereas partial-span suction is of limited value. For the full-span suction condition and high suction flow rates (figs. 15 and 21), maximum lift values of 3.9 and 2.1 were measured for the rough surface condition with the flaps deflected 45° and 0°, respectively.

Lift-drag ratios.- The evaluation of wing lift-drag ratios is always a problem which requires extreme care inasmuch as wing absolute drag values

(with all tunnel corrections) must be very accurately determined. As the basic purpose of the investigation in the Langley full-scale tunnel involved the determination of wing lift-drag ratios, extreme care was taken in evaluating stream angle, blower tares, and other tunnel corrections. Profile-drag surveys (figs. 16 and 17) using the wake-momentum method were made to furnish a check against force data. A comparison of profile-drag data obtained from momentum surveys and computed from force data is presented in figure 18. Good agreement between the two methods of measurement is indicated for all conditions at which comparisons are made. The momentum-survey data are also useful for estimating the increment of wing drag resulting from interference at the juncture of the wing and reflection plane.

Figures 22 and 23 present the lift-drag-ratio characteristics of the aspect-ratio-20 wing tested in Langley full-scale tunnel (model I) for several wing configurations including the effects of slot configuration, flap installation, and leading-edge roughness. Data are presented for only the more nearly optimum flow rates for each configuration and are computed from force data which include the wing-root interference drag. These data show that the optimum slot arrangement tested was the tapered inboard 0.52 b/2 slot which, for the smooth-wing configuration with landing flaps installed, reached a maximum lift-drag ratio of 26 as compared to 24 for the full-span, constant-1.5-percent-chord slot. For all slot configurations, maximum lift-drag-ratio values were reached at a lift coefficient ranging from 0.9 to 1.0; these values are in good agreement with predictions based on two-dimensional tests (ref. 1).

Lift-drag ratios for model II are presented in figure 29 to illustrate the order of magnitude of Mach number and surface roughness effects on the maximum lift-drag-ratio characteristics for a wing of this type. These results show that increasing the Mach number from 0.2 to 0.44 reduced the maximum lift-drag ratio by less than 1 for either the smooth- or rough-model configurations. Installing leading-edge roughness reduced the maximum lift-drag-ratio values by approximately 2 throughout the Mach number range (compare figs. 29(a) and 29(b)), although, as was previously described, it was necessary to increase the suction flow rate slightly to obtain maximum lift-drag ratio at the higher Mach numbers.

In order to gain a better indication of the maximum lift-drag ratios obtained for the aspect-ratio-20 wing, the data for model I have been corrected for the increment of wing-root interference drag indicated by the momentum surveys. The resulting lift-drag ratios for the wing without flaps are shown in figure 24 as a function of lift coefficient. The results for the semispan slot configuration without flaps were inferred from tests of the wing with flaps installed by using flap drag increments measured on the wing with the full-span slot.

The results shown in figure 24 indicate that the maximum values of the lift-drag ratio obtained for model I in the smooth condition were

30.8 for the 2- to 0-percent chord, tapered-slot configuration and 27.2 for the configuration with the full-span, 1.5-percent-chord slot. In the rough-leading-edge condition, the maximum lift-drag ratio was 25.2 for the configuration with the full-span, 1.5-percent-chord slot. No data were obtained for the 2- to 0-percent-chord, tapered-slot configuration with leading-edge roughness. Unfortunately, it is not possible on the basis of the data presented in figure 24 to state with certainty whether the values of lift-drag ratio predicted by the analysis of reference 1 can be realized on an actual three-dimensional wing. The predicted values of lift-to-drag ratio given in reference 1 are for untwisted wings in the rough-surface condition. In all cases, the optimum flow removal for minimum total drag was assumed at all points along the span. The maximum value of lift-drag ratio predicted for an aspect-ratio-20 wing with 0.3 taper ratio was about 29, which is, of course, considerably higher than the value of 25.2 obtained experimentally for the rough-leading-edge condition in the present investigation. On the other hand, altering the slot design in such a way as to obtain a more favorable spanwise distribution of suction is seen from figure 24 to increase the lift-drag ratio of the smooth wing from 27.2 to 30.8. One might infer, therefore, that, had the model in the rough-leading-edge condition been tested with a slot design more nearly optimum than the full-span, 1-percent-chord slot, values of the lift-drag ratio considerably in excess of 25.2 might have been obtained.

In order to obtain some indication of the manner in which the lift-drag ratios of the aspect-ratio-20 wing compare with those of a wing of more conventional design, a study was made of the results contained in references 7 and 8 for a number of full-span, three-dimensional wings. The wings for which data are given in references 7 and 8 had various plan forms and airfoil sections, but all had a span-to-root thickness ratio of 35. Of the wings investigated with a taper ratio near 0.286, an aspect-ratio-12 wing having a taper ratio of 0.286 and NACA 44 series airfoil sections was chosen as a basis for comparison with the aspect-ratio-20 wing of the present investigation. This particular wing was chosen since it appeared to have about the highest lift-drag ratio in the rough-surface condition of any of the wings investigated with taper ratios near 0.286. The data for this wing at a Reynolds number of 2.8×10^6 indicate maximum lift-drag-ratio values of 24.5 and 33 for the leading-edge-rough and leading-edge-smooth conditions, respectively.

Because of differences in model surface condition, it is difficult to draw any conclusions from a comparison of the maximum lift-drag ratios of the wings without leading-edge roughness. In the rough-leading-edge condition, however, a more sound basis of comparison exists. For this condition, the maximum lift-drag ratios of the two wings are not greatly different, although that of the aspect-ratio-20 wing is slightly higher than that of the aspect-ratio-12 wing. In accordance with the previous discussion of the effects of slot design on the maximum lift-drag ratio,

however, it seems possible that, with a more nearly optimum slot design, the aspect-ratio-20 wing might show a more pronounced advantage over the aspect-ratio-12 wing in the rough surface condition. It is perhaps worthy of note that the lift coefficient for maximum lift-drag ratio is much higher for the aspect-ratio-20 wing than for the aspect-ratio-12 wing.

CONCLUSIONS

An investigation of an aspect-ratio-20, straight wing equipped with a suction slot to eliminate separation of the boundary layer near the trailing edge indicates the following conclusions:

1. Trailing-edge separation on the thick root sections of a wing of the type investigated may be effectively controlled through boundary-layer suction. Unless the suction flow rates at each local station across the span are carefully limited to the minimum requirement for each section, however, wing total-drag coefficients including blower power will be excessive.

2. From a consideration of obtaining minimum total-drag and maximum lift-drag ratios in the lift-coefficient range from 0.4 to 1.0, a tapered slot on the inboard 0.52 semispan portion of the wing appears to be a more nearly optimum arrangement than a full-span slot of constant-percent-chord width.

3. For maximum lift, the full-span suction-slot configuration is much more effective than the 0.52 semispan suction configuration. With full-span trailing-edge flaps installed and maximum suction rates in the full-span slot, maximum lift values of 4.2 and 2.5 were obtained for the flaps-deflected and flaps-neutral configuration, respectively.

4. The maximum values of the lift-drag ratio obtained for the wing in the leading-edge-smooth and leading-edge-rough surface conditions were 30.8 and 25.2, respectively. The decrement in lift-drag ratio between 30.8 and 25.2 is not due entirely to leading-edge roughness, however, since the full-span constant-1.5-percent-chord slot was employed on the roughened wing, whereas the more nearly optimum tapered slot was employed on the smooth wing.

5. No adverse effects of compressibility were observed through the Mach number range investigated (maximum Mach number of 0.44) for lift coefficients up to and including 1.0.

Langley Aeronautical Laboratory,
National Advisory Committee for Aeronautics,
Langley Field, Va., May 8, 1953.

REFERENCES

1. Horton, Elmer A., Racisz, Stanley F., and Paradiso, Nicholas J.: Investigation of NACA 64,2-432 and 64,3-440 Airfoil Sections With Boundary-Layer Control and an Analytical Study of Their Possible Applications. NACA TN 2405, 1951.

2. Anderson, Raymond F.: Determination of the Characteristics of Tapered Wings. NACA Rep. 572, 1936.

3. Von Doenhoff, Albert E., and Horton, Elmer A.: Wind-Tunnel Investigation of NACA 65,3-418 Airfoil Section With Boundary-Layer Control Through a Single Suction Slot Applied to a Plain Flap. NACA RM L9A20, 1949.

4. Goett, Harry J.: Experimental Investigation of the Momentum Method for Determining Profile Drag. NACA Rep. 660, 1939.

5. Von Kármán, Th.: Compressibility Effects in Aerodynamics. Jour. Aero. Sci., vol. 8, no. 9, July 1941, pp. 337-356.

6. Horton, Elmer A., Racisz, Stanley F., and Paradiso, Nicholas J.: Investigation of Boundary-Layer Control To Improve the Lift and Drag Characteristics of the NACA 65_2-415 Airfoil Section With Double Slotted and Plain Flaps. NACA TN 2149, 1950.

7. Neely, Robert H., Bollech, Thomas V., Westrick, Gertrude C., and Graham, Robert R.: Experimental and Calculated Characteristics of Several NACA 44-Series Wings With Aspect Ratios of 8, 10, and 12 and Taper Ratios of 2.5 and 3.5. NACA TN 1270, 1947.

8. Bollech, Thomas V.: Experimental and Calculated Characteristics of Several High-Aspect-Ratio Tapered Wings Incorporating NACA 44-Series, 230-Series, and Low-Drag 64-Series Sections. NACA TN 1677, 1948.

TABLE I

BASIC AIRFOIL ORDINATES FOR ASPECT-RATIO-20 WING

[Stations and ordinates are in percent of airfoil chord]

NACA 64,2-437, a = 1 (modified) airfoil section				NACA 645-424 airfoil section			
Upper surface		Lower surface		Upper surface		Lower surface	
Station	Ordinate	Station	Ordinate	Station	Ordinate	Station	Ordinate
0	0	0	0	0	0	0	0
-.012	3.843	1.012	-3.705	.195	1.912	.805	-1.712
.143	4.648	1.357	-4.442	.410	2.328	1.090	-2.048
.511	5.879	1.989	-5.543	.863	2.995	1.637	-2.567
1.578	8.048	3.422	-7.400	2.048	4.249	2.952	-3.505
3.950	10.966	6.050	-9.768	4.485	6.126	5.515	-4.862
6.453	13.041	8.547	-11.377	6.963	7.566	8.037	-5.870
9.008	14.632	10.992	-12.576	9.461	8.741	10.539	-6.673
14.138	16.952	15.862	-14.260	14.489	10.610	15.511	-7.918
19.253	18.536	20.747	-15.352	19.541	12.000	20.459	-8.816
24.377	19.607	25.623	-16.027	24.607	13.014	25.393	-9.434
29.506	20.270	30.494	-16.382	29.683	13.692	30.317	-9.804
34.636	20.556	35.364	-16.436	34.764	14.045	35.236	-9.925
39.764	20.470	40.236	-16.186	39.846	14.048	40.154	-9.764
44.887	19.941	45.113	-15.561	44.927	13.600	45.073	-9.220
50.000	18.980	50.000	-14.568	50.000	12.875	50.000	-8.463
55.098	17.628	54.902	-13.248	55.062	11.929	54.938	-7.549
60.178	15.942	59.822	-11.658	60.112	10.801	59.888	-6.517
65.235	13.990	64.765	-9.870	65.147	9.530	64.853	-5.410
70.267	11.855	69.733	-7.967	70.168	8.154	69.832	-4.266
75.274	9.632	74.726	-6.052	75.172	6.712	74.828	-3.132
80.257	7.411	79.743	-4.227	80.161	5.241	79.839	-2.057
85.216	5.251	84.784	-2.559	85.135	3.791	84.865	-1.099
90.152	3.205	89.848	-1.137	90.096	2.402	89.904	-.334
95.073	1.413	94.927	-.149	95.046	1.124	94.954	.140
100.000	0	100.000	0	100.000	0	100.000	0
L.E. radius: 14.260				L.E. radius: 3.50			

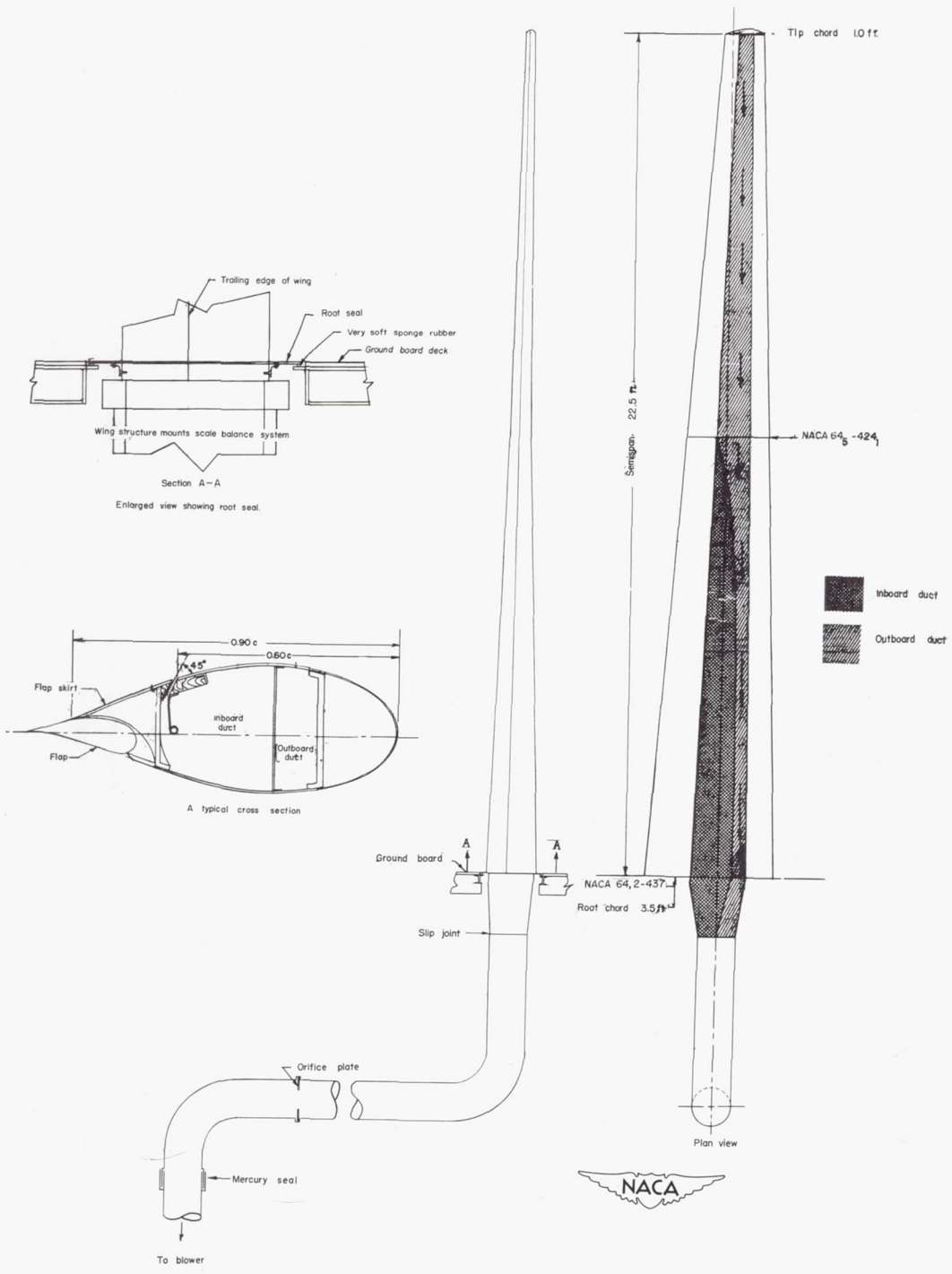


TABLE II

BASIC FLAP ORDINATES FOR ASPECT-RATIO-20 WING

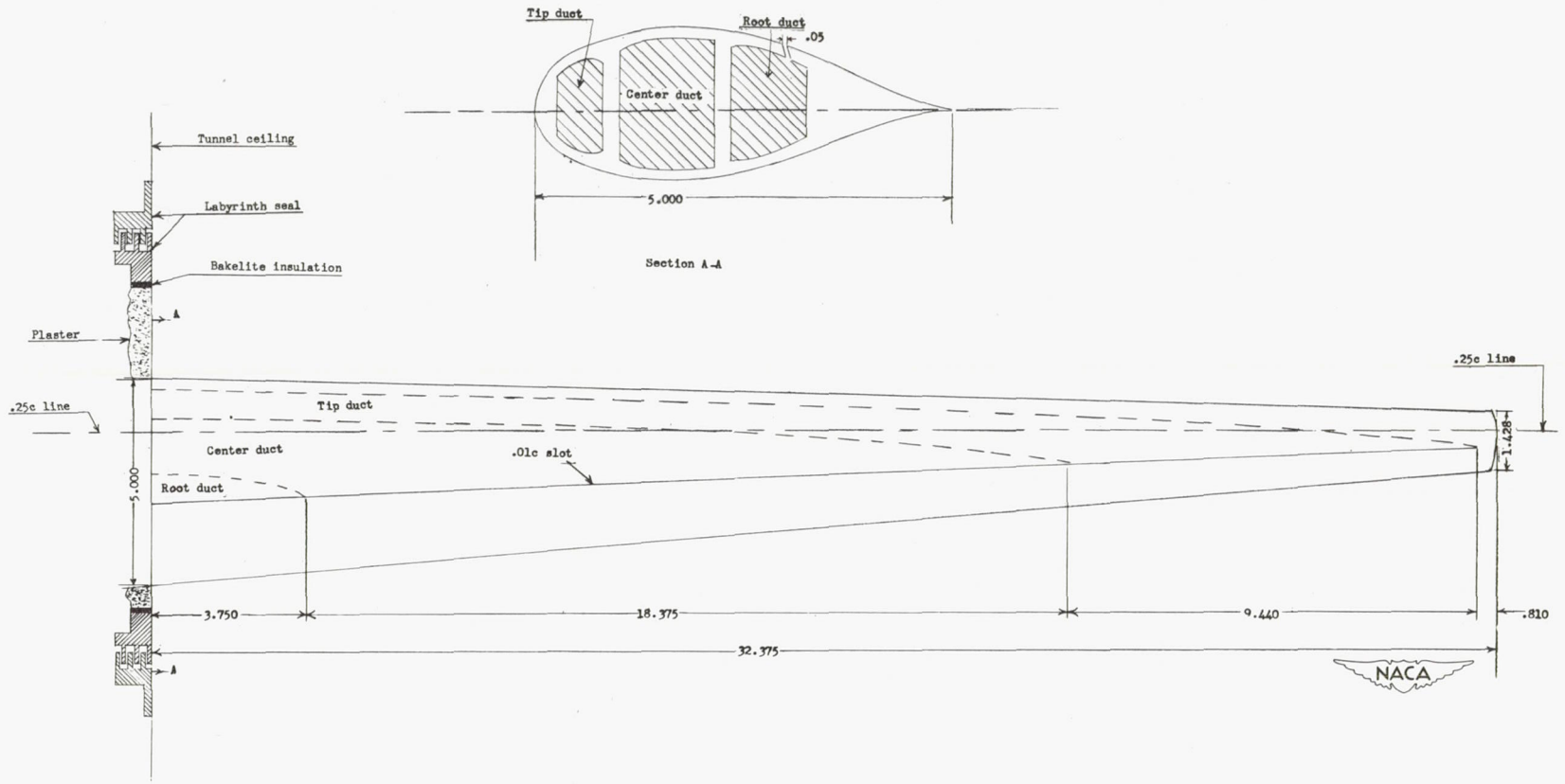
[Stations and ordinates are in percent airfoil chord]

NACA 64,2-437 airfoil section				NACA 645-424 airfoil section			
Upper surface		Lower surface		Upper surface		Lower surface	
Station	Ordinate	Station	Ordinate	Station	Ordinate	Station	Ordinate
70.000	-2.000	70.000	-2.000	70.000	-1.665	70.000	-1.665
70.250	-.390	70.250	-3.390	70.208	-.624	70.833	-3.230
70.500	.265	70.500	-3.935	70.500	0	72.918	-3.542
71.000	1.190	71.000	-4.630	70.833	.417	77.085	-2.623
72.000	2.390	72.000	-5.465	71.875	1.457	83.340	-1.416
74.000	3.860	74.000	-6.000	72.918	2.167	87.500	-.667
		76.000	-5.560	75.000	2.960	91.770	-.083
76.000	4.630	79.743	-4.227	79.175	3.542	95.820	.188
79.000	5.035	84.784	-3.559	83.340	3.438	100.000	0
83.000	4.855	89.848	-1.137	89.580	2.396		
87.000	4.065	94.927	-.149	95.820	.937		
91.000	2.855	100.000	0	100.000	0		
95.073	1.413						
100.000	0						
L.E. radius: 4.00 Location of L.E. radius center: 74.00				L.E. radius: 1.660			



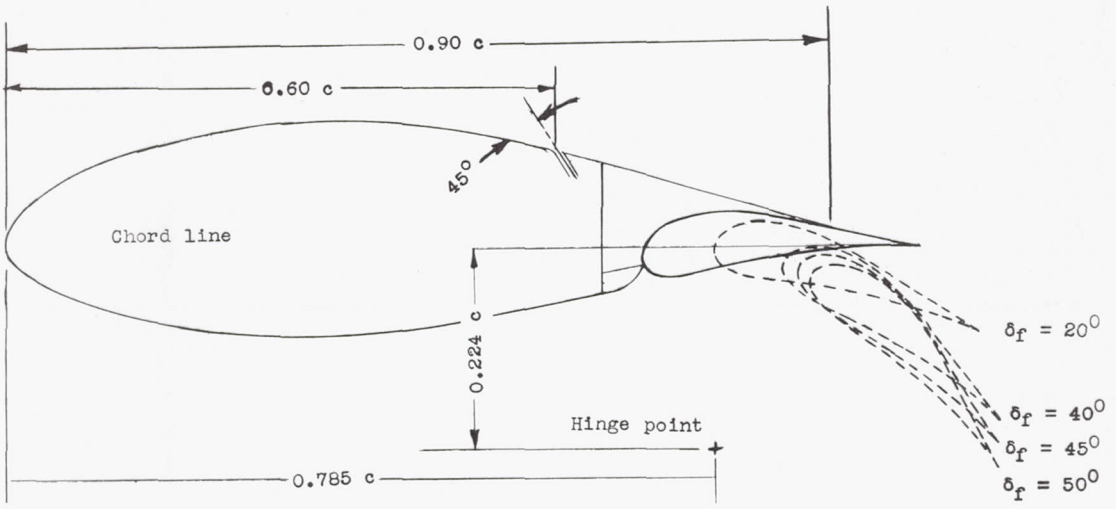
(a) Model I.

Figure 1.- General layout and principal dimensions of aspect-ratio-20 boundary-layer model. A typical cross section and a sketch of the root seal are also shown.

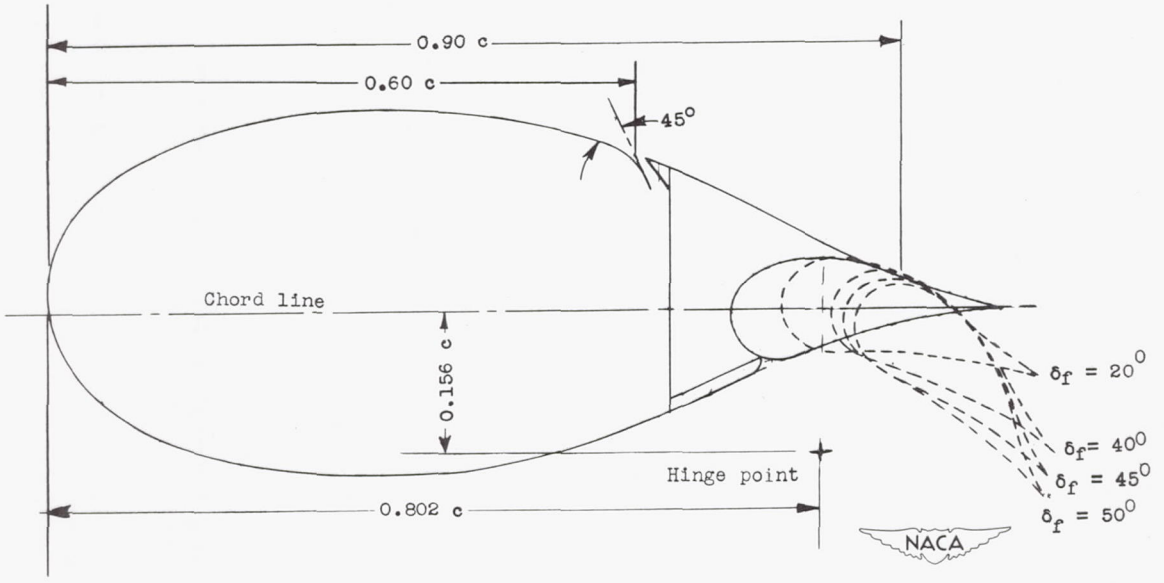


(b) Plan form of model showing general ducting and root cross section. Model II. All dimensions are in inches.

Figure 1.- Concluded.

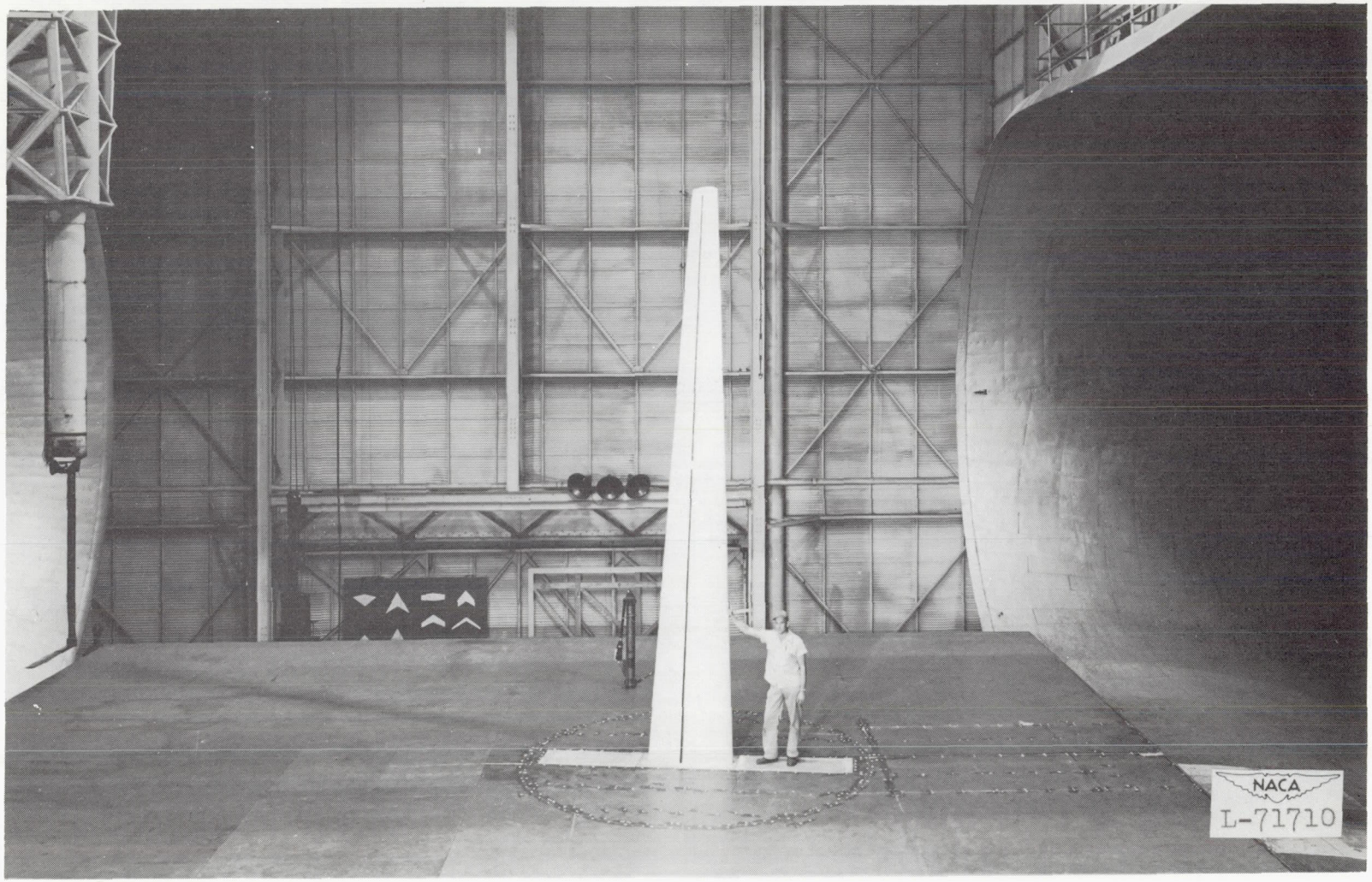


(a) NACA 64_5-424 airfoil section.



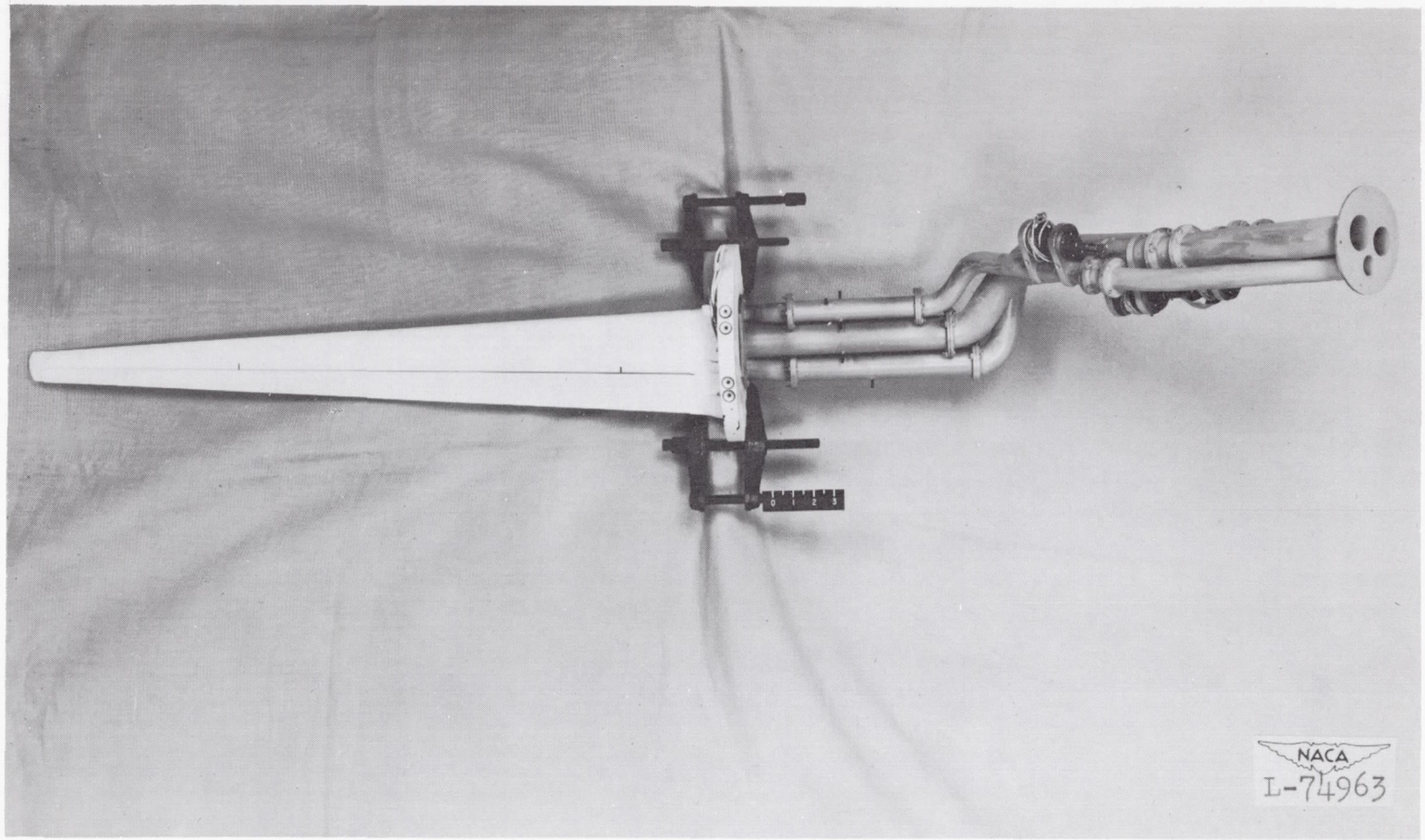
(b) NACA 64,2-437 airfoil section.

Figure 2.- Profiles of the NACA 64_5-424 and the NACA 64,2-437 airfoil sections showing slot and flap-hinge location and flap deflection.



(a) Model I mounted in Langley full-scale tunnel.

Figure 3.- Photographs of aspect-ratio-20 boundary-layer wing.



(b) Model II showing ducting arrangement.

Figure 3.- Concluded.

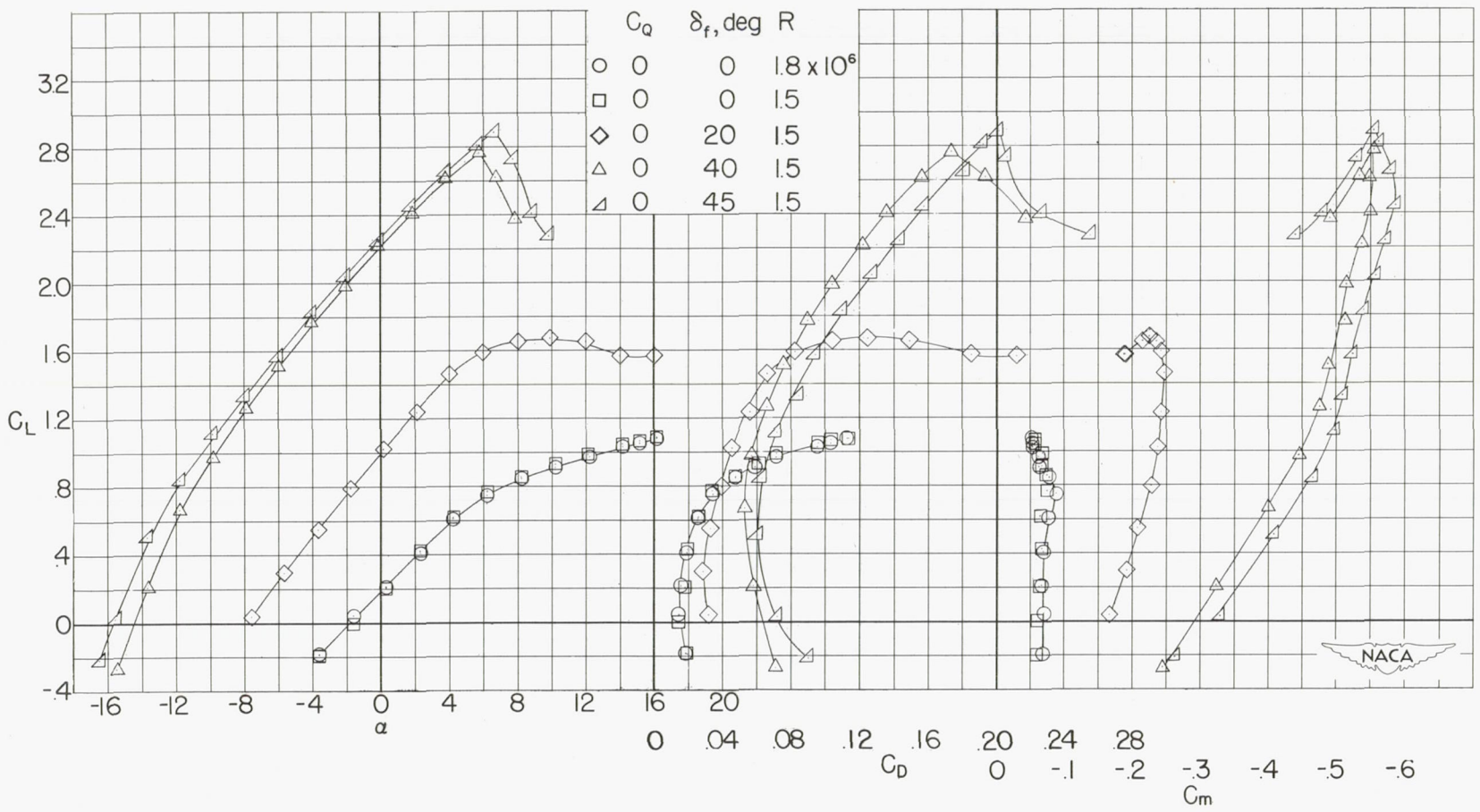
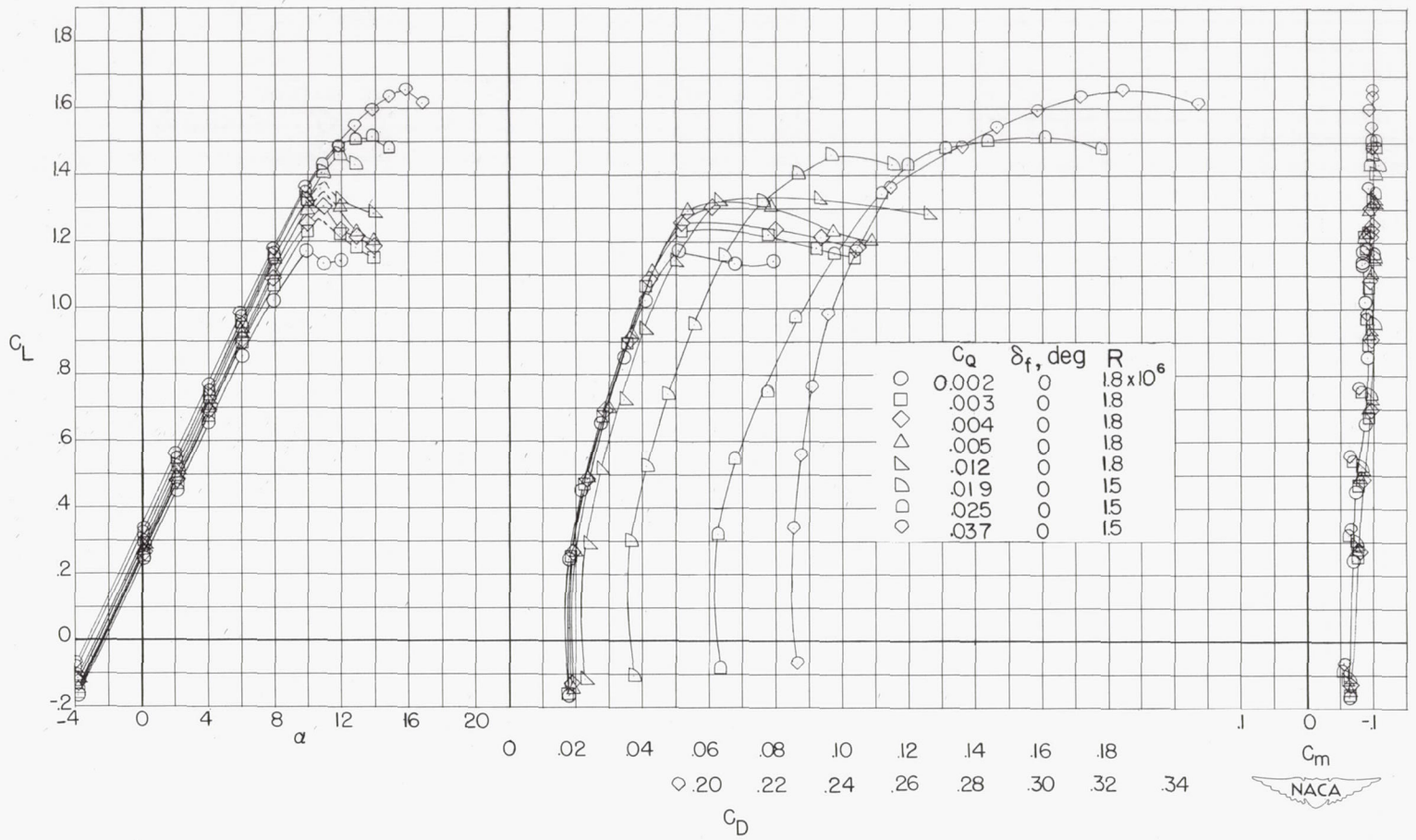
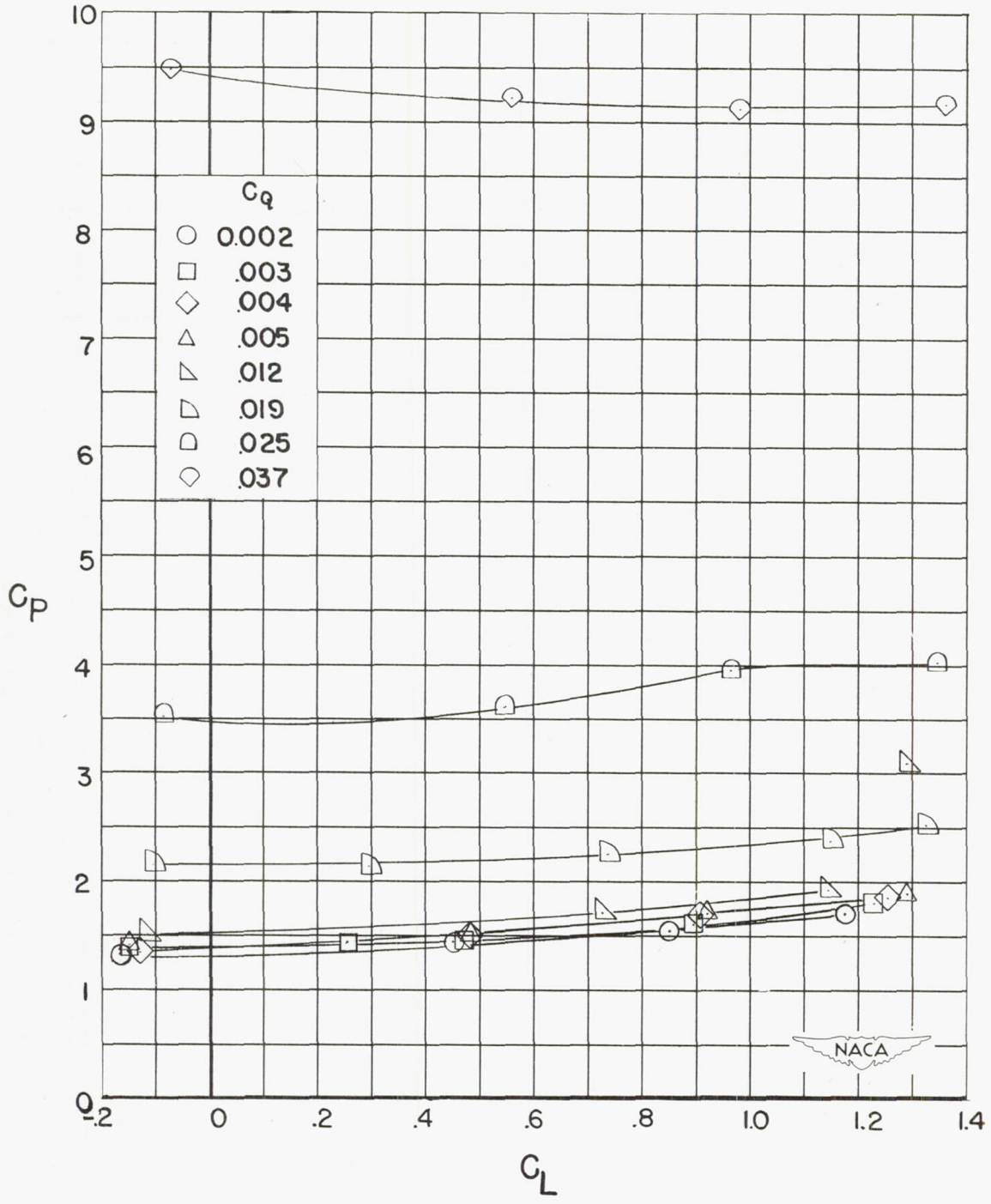


Figure 4.- Aerodynamic characteristics of the basic wing. Suction slot sealed and faired; flaps installed; wing smooth; model I.



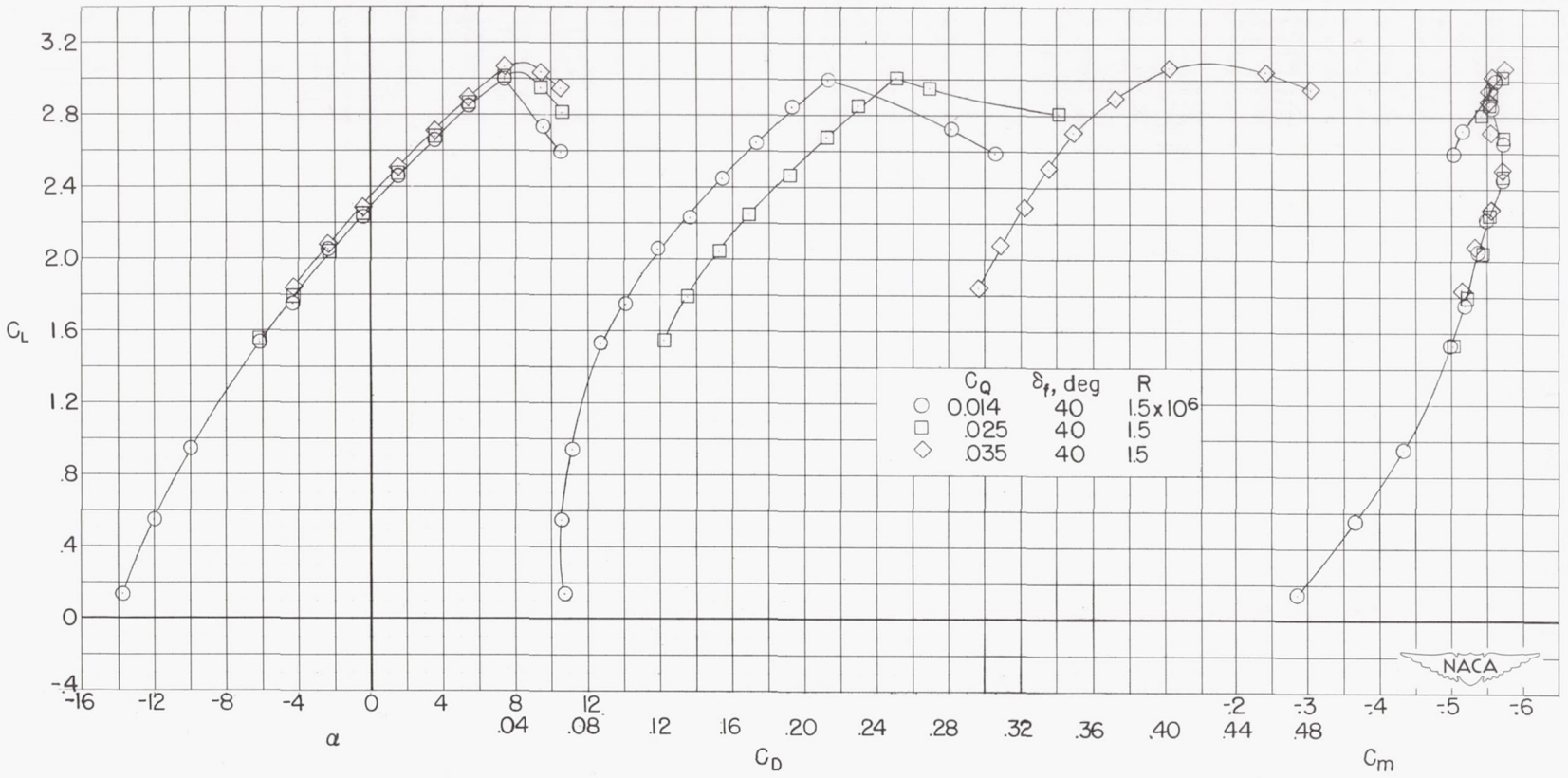
(a) Variation of C_L with α, C_D, and C_m.

Figure 5.- Aerodynamic characteristics of the wing with suction applied to inboard semispan only. Inboard semispan slot tapered from 2 to 0 percent chord. Wing smooth; model I. Note that C_D values for C_Q of 0.037 are plotted on a different scale.



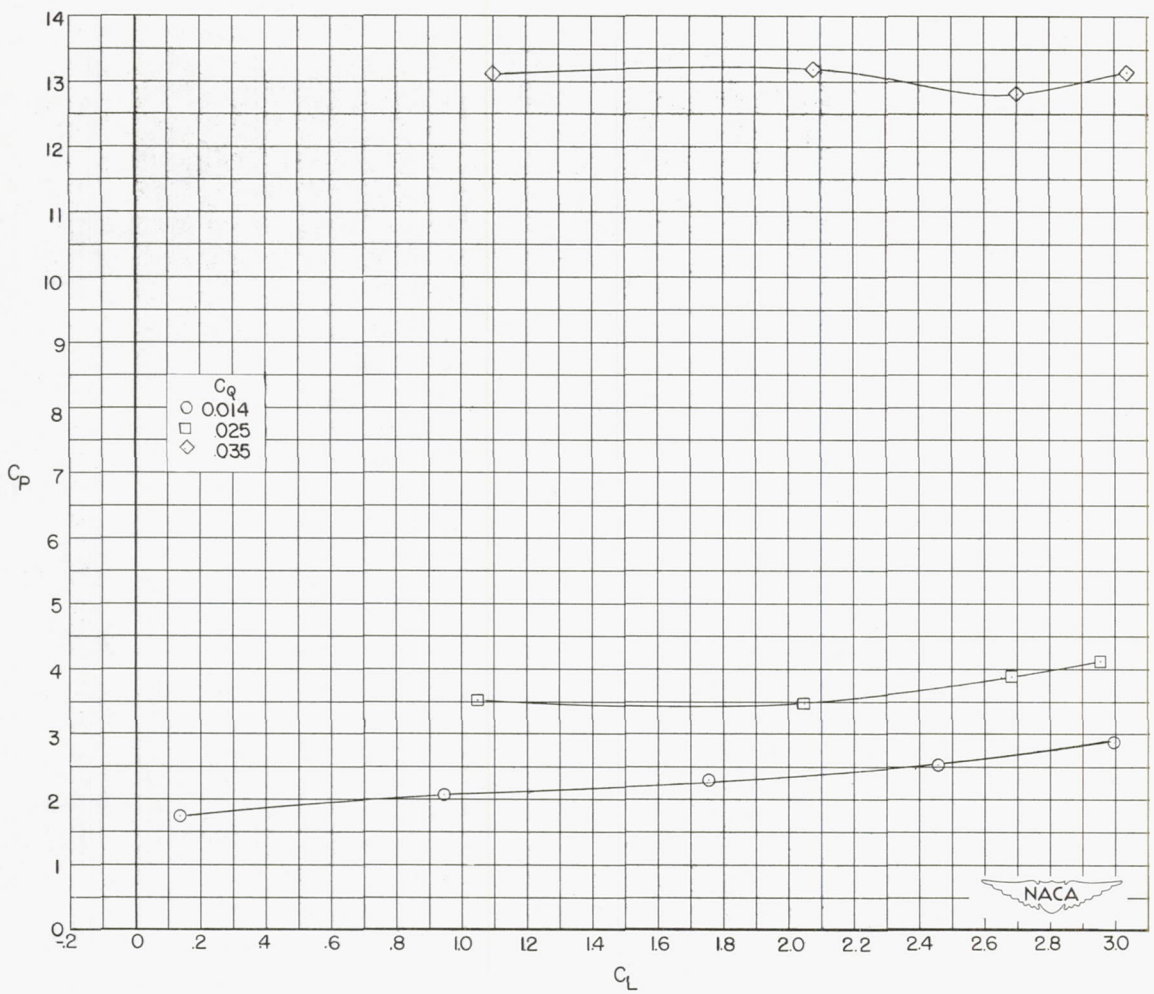
(b) Variation of pressure-loss coefficient with lift coefficient.

Figure 5.- Concluded.



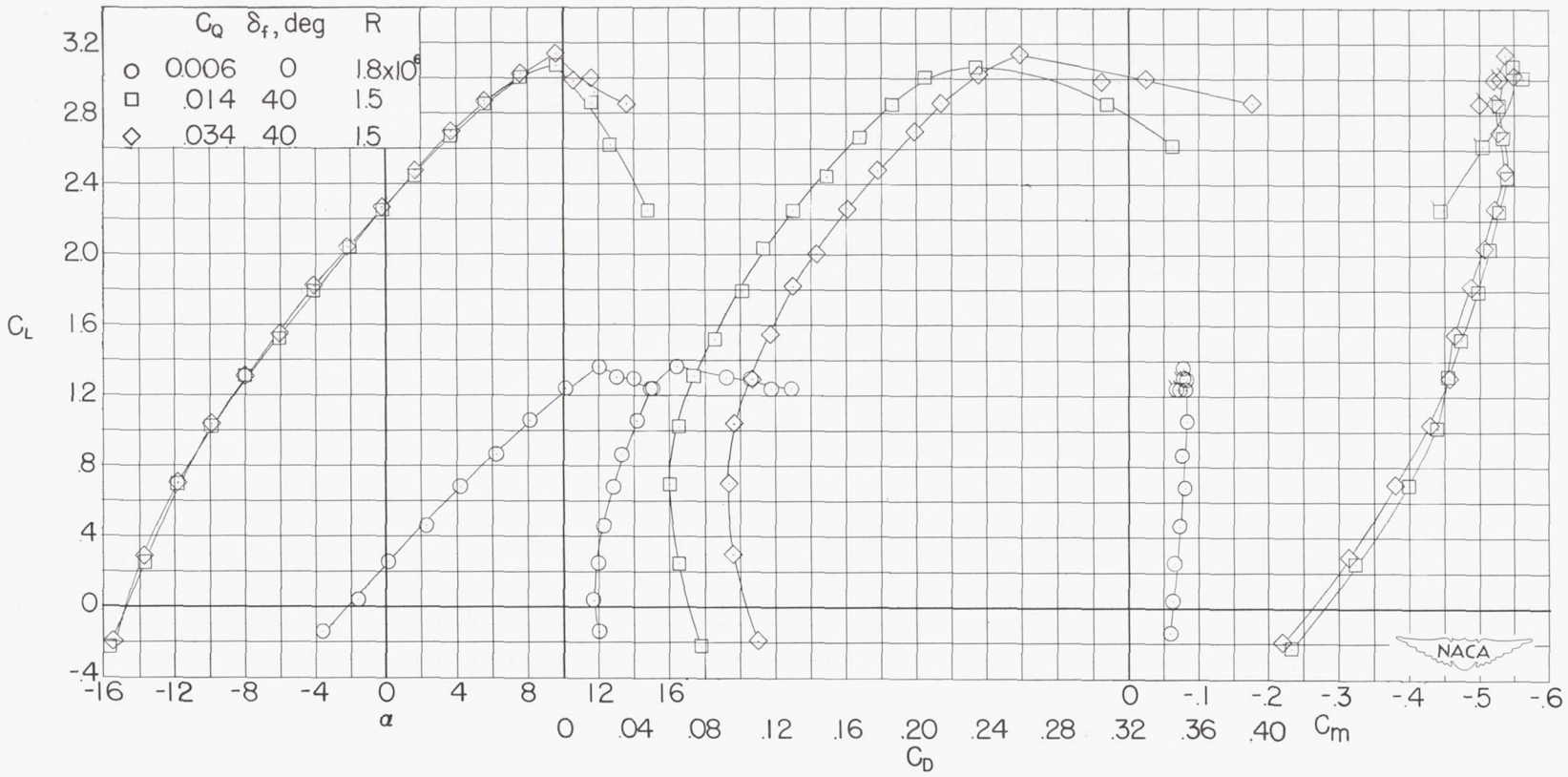
(a) Variation of C_L with α, C_D, and C_m.

Figure 6.- Aerodynamic characteristics of the wing with suction applied to inboard semispan only. Inboard semispan slot tapered from 2 to 0 percent chord; full-span flaps deflected 40°; wing smooth; model I.



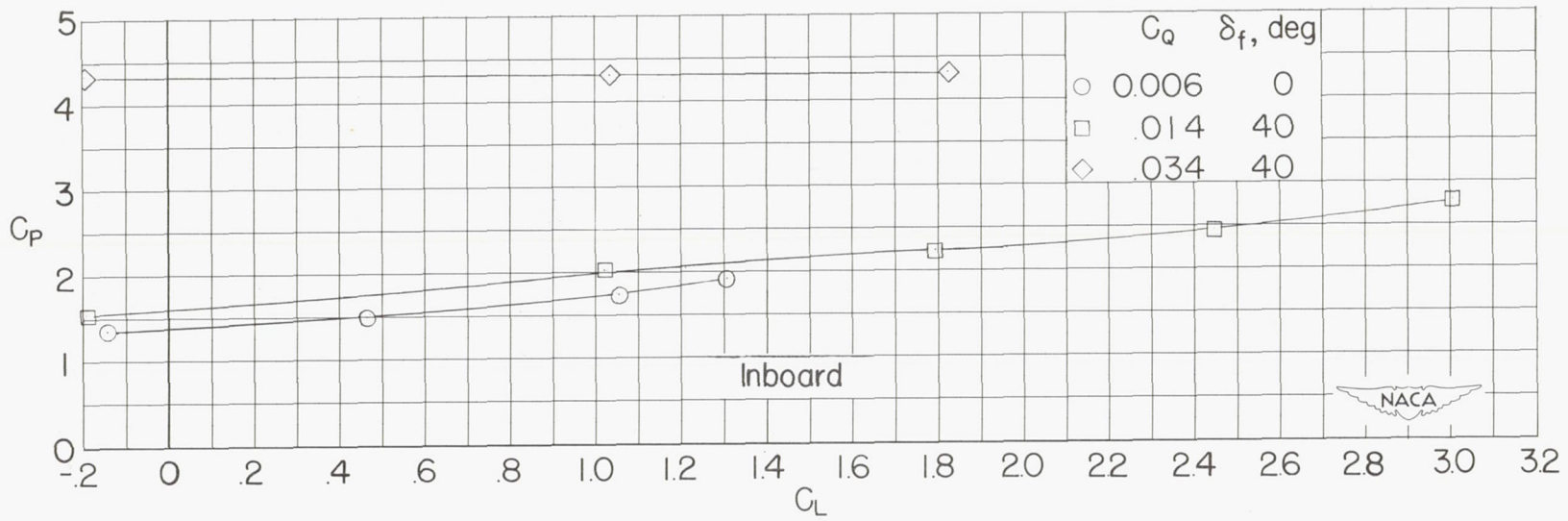
(b) Variation of pressure-loss coefficient with lift coefficient.

Figure 6.- Concluded.



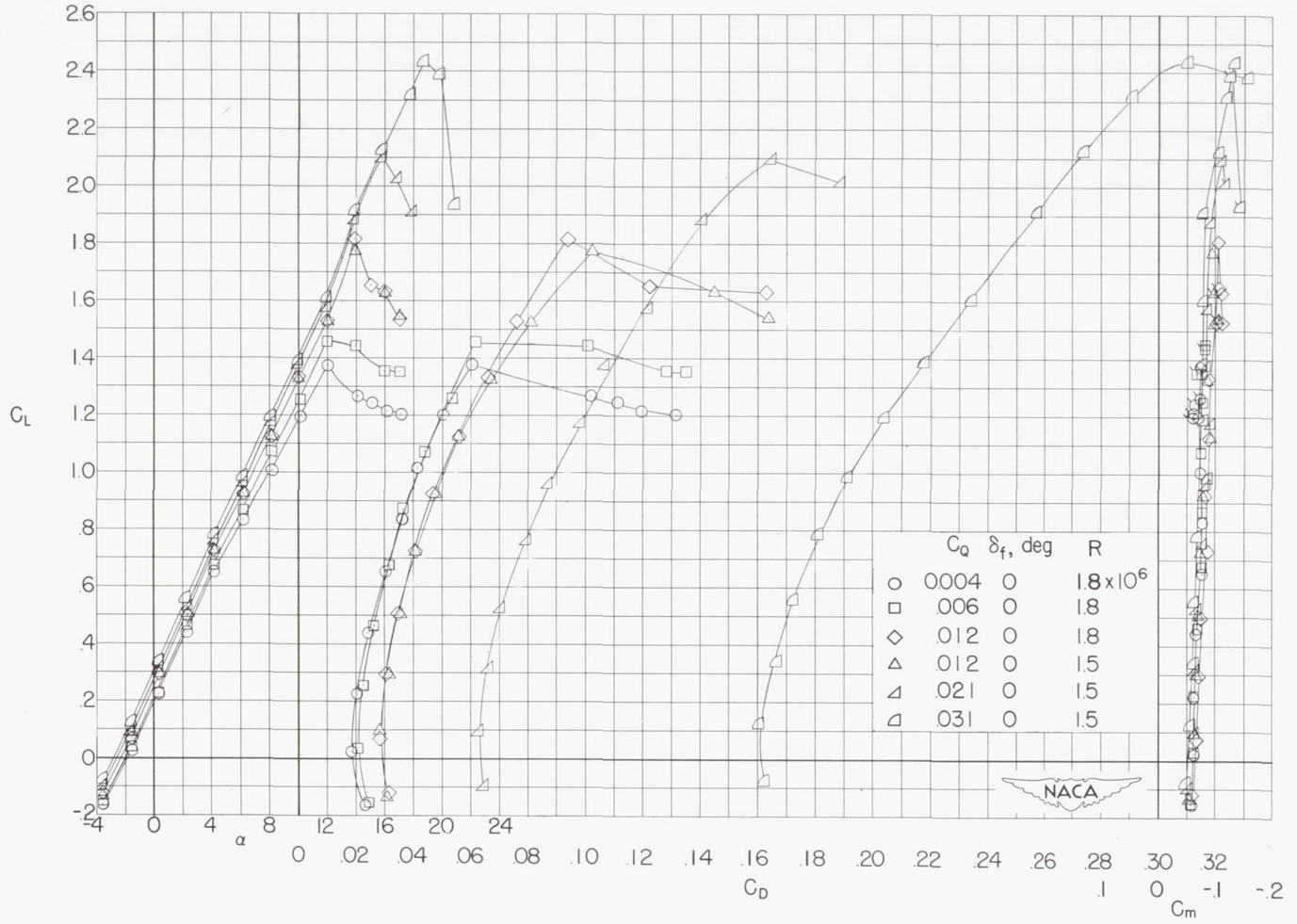
(a) Variation of C_L with α, C_D, and C_m.

Figure 7.- Aerodynamic characteristics of the wing with suction applied to inboard semispan only. Flaps installed; inboard semispan slot constant 1 percent chord; model I.



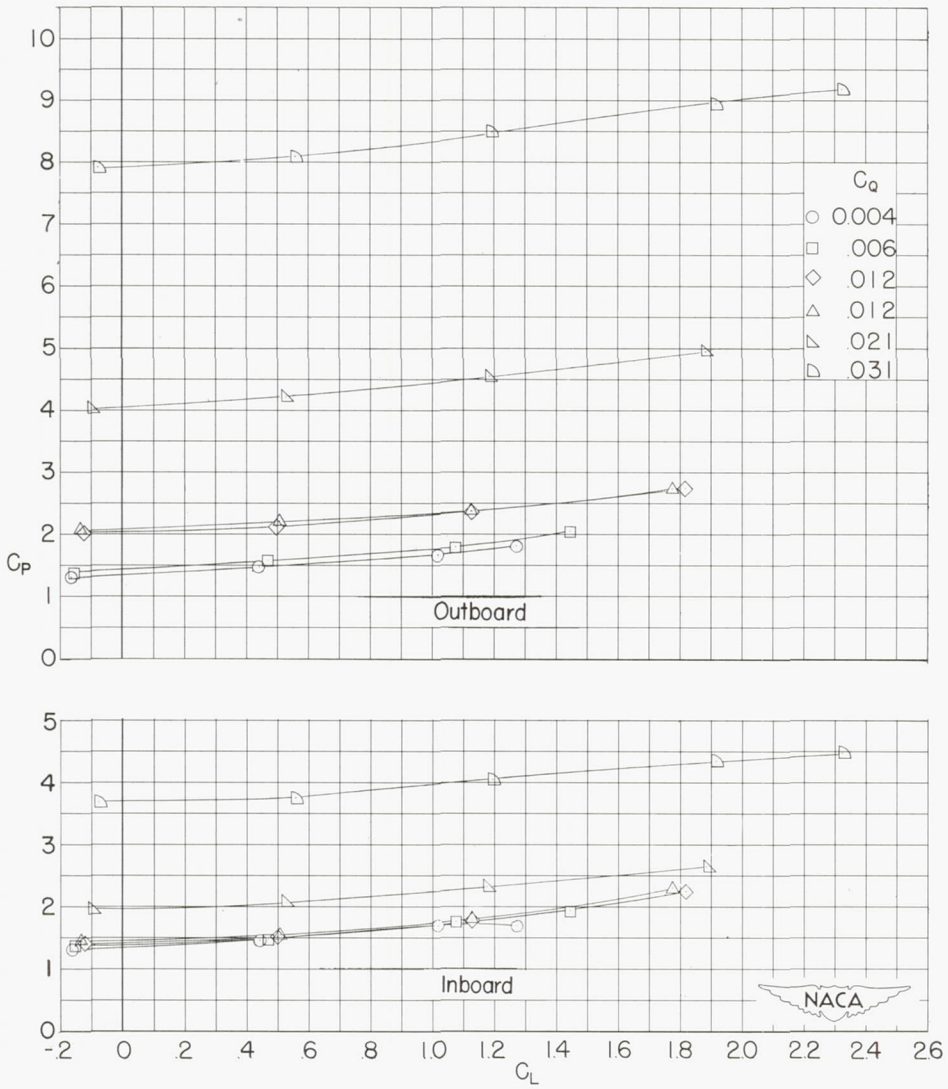
(b) Variation of pressure-loss coefficient with lift coefficient.

Figure 7.- Concluded.



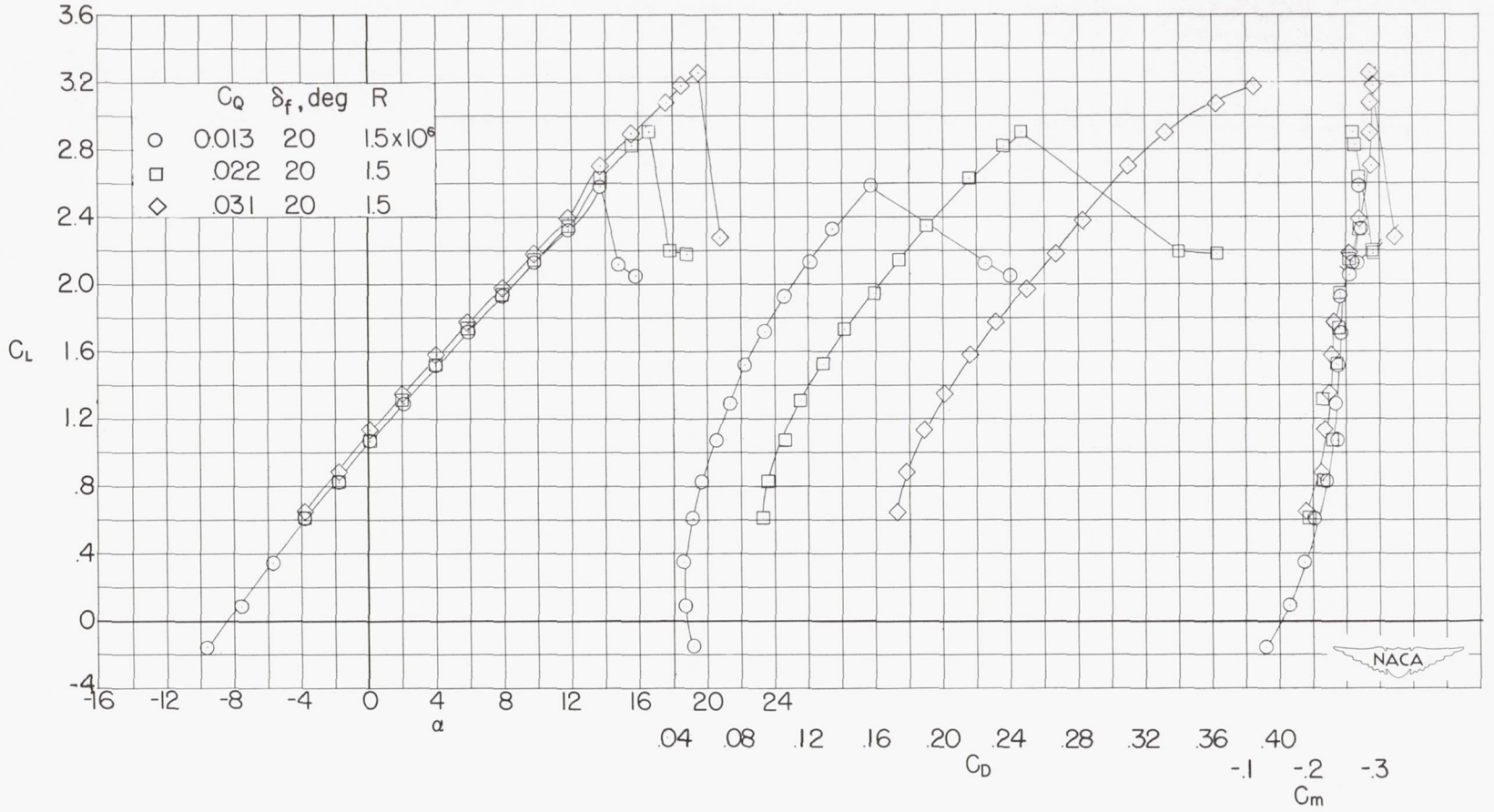
(a) Variation of C_L with α, C_D, and C_m.

Figure 8.- Aerodynamic characteristics of the wing with suction applied full span. Flaps installed; wing smooth; model I.



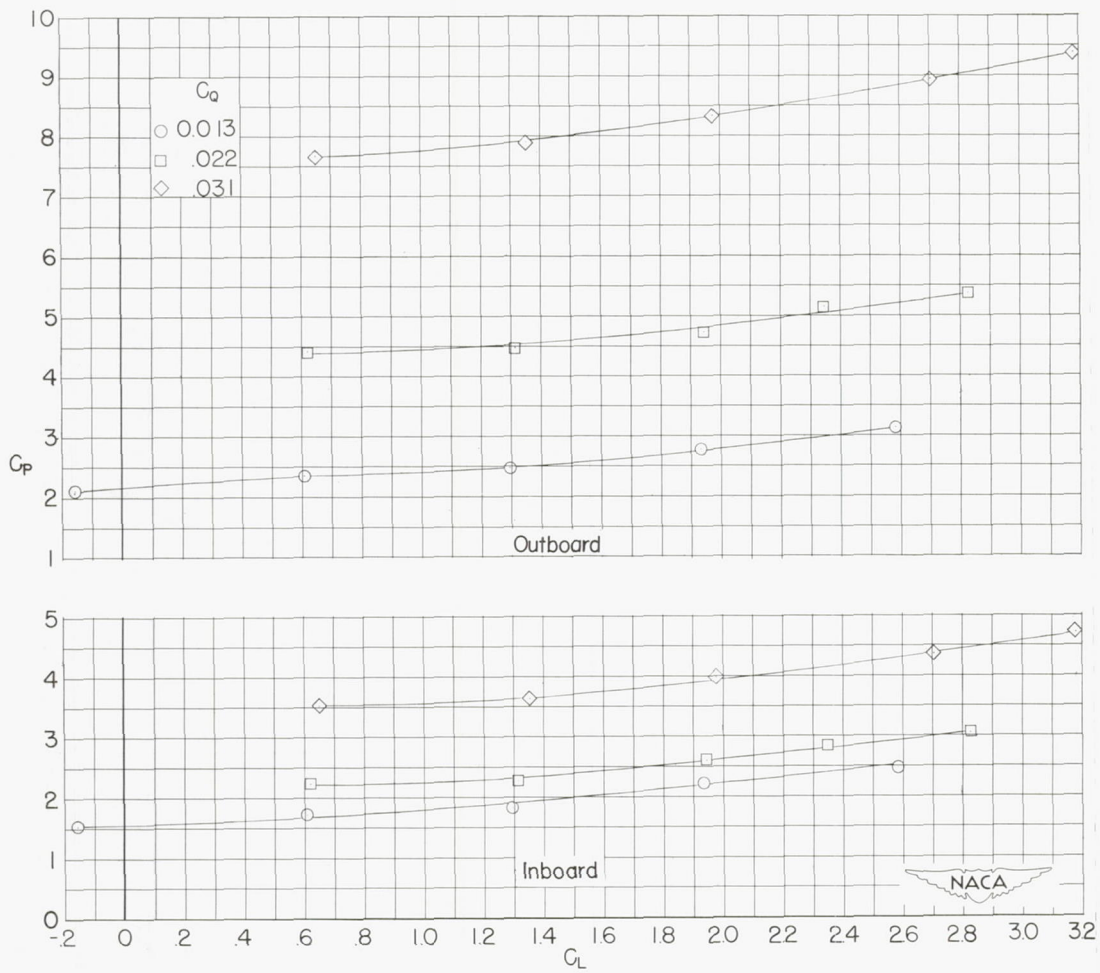
(b) Variation of pressure-loss coefficient with lift coefficient.

Figure 8.- Concluded.



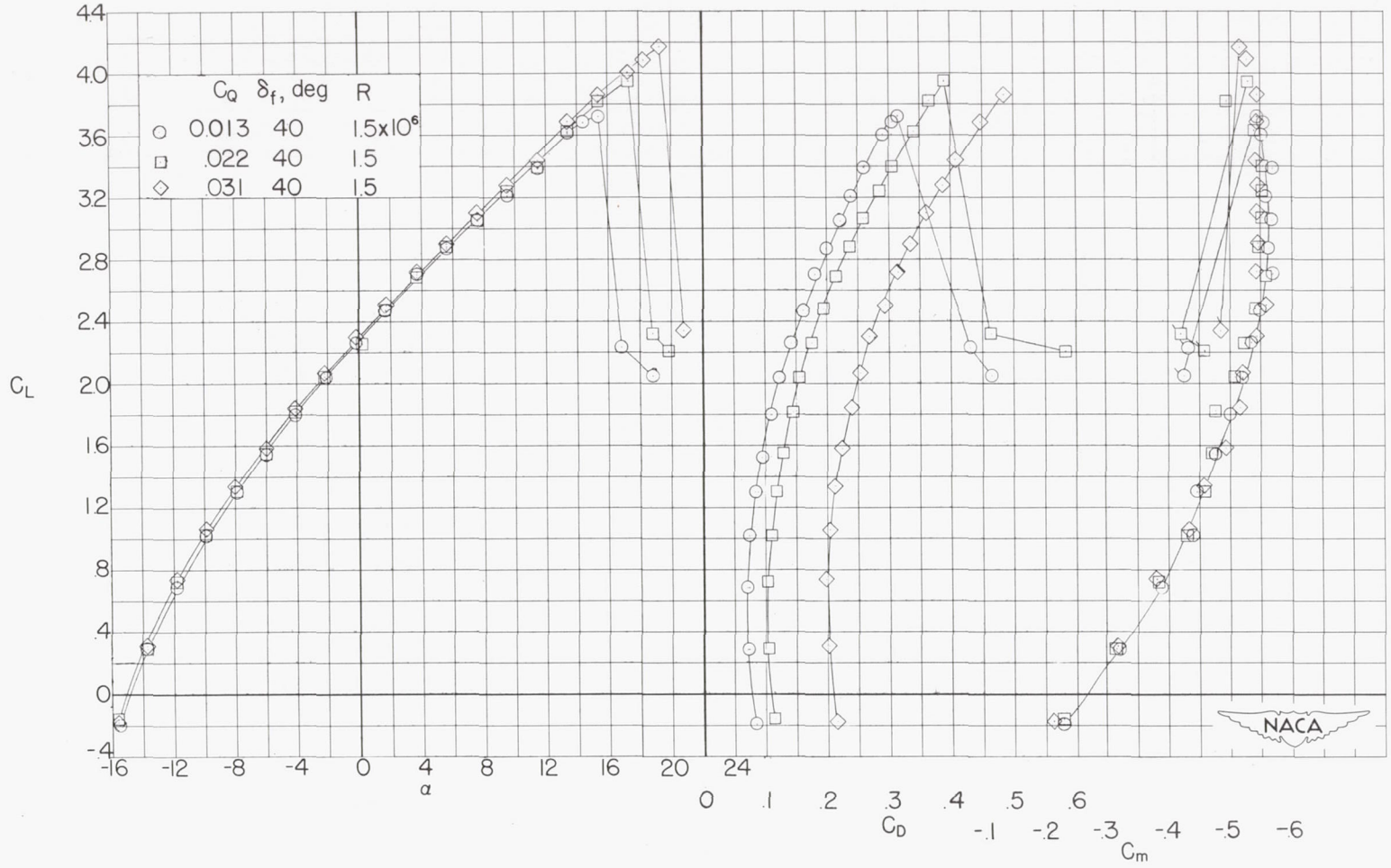
(a) Variation of C_L with α, C_D, and C_m.

Figure 9.- Aerodynamic characteristics of the wing with suction applied full span. Flaps deflected 20°; wing smooth; model I.



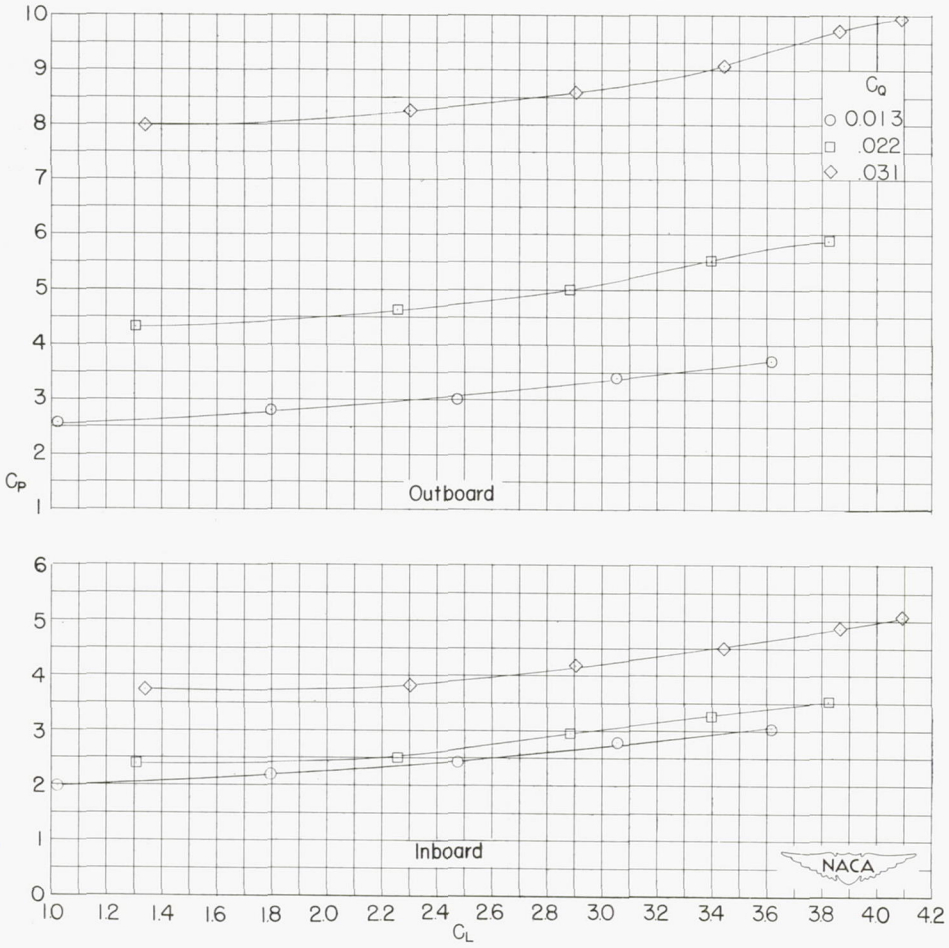
(b) Variation of pressure-loss coefficient with lift coefficient.

Figure 9.- Concluded.



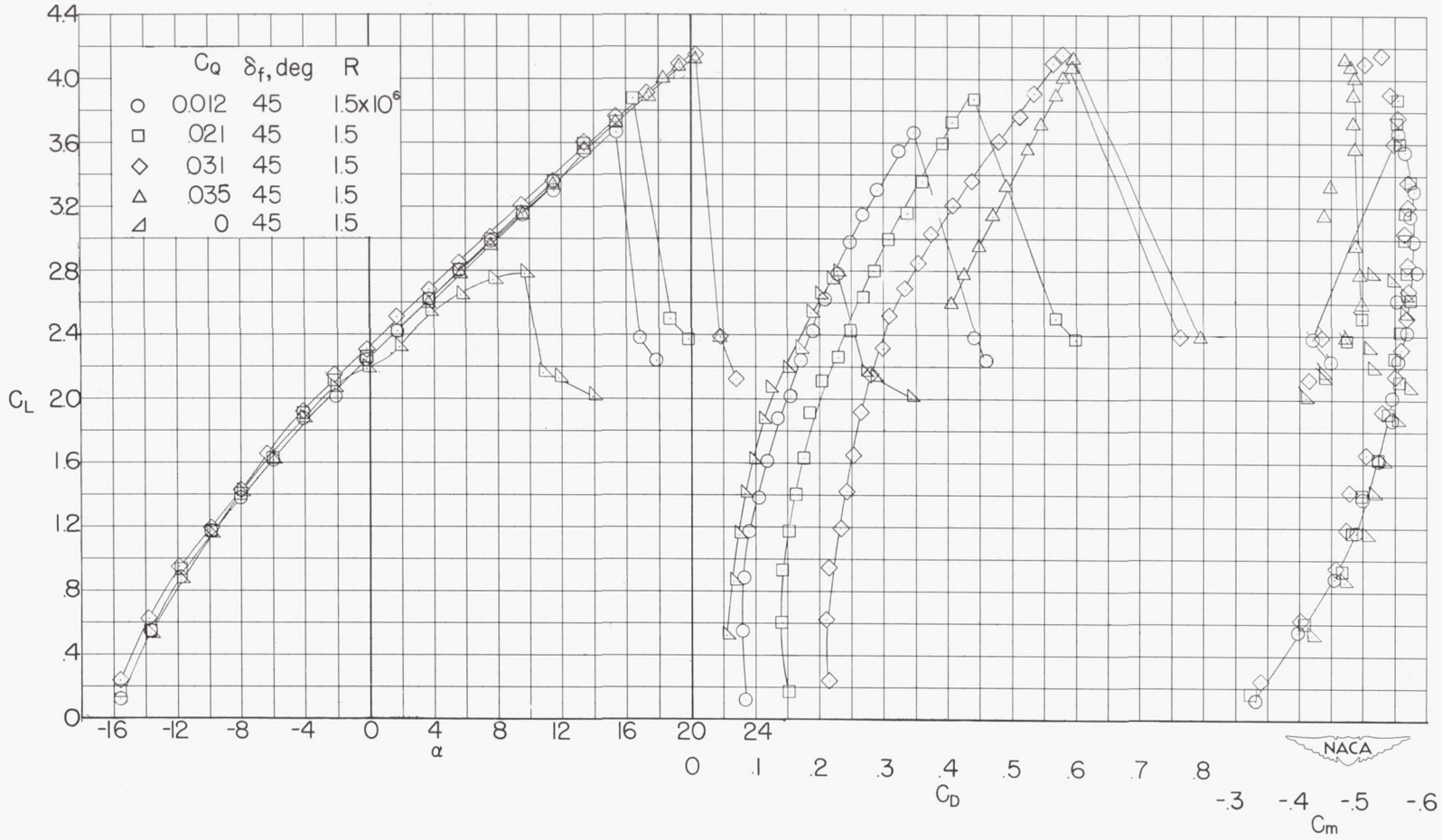
(a) Variation of C_L with α, C_D, and C_m.

Figure 10.- Aerodynamic characteristics of the wing with suction applied full span. Flaps deflected 40°; wing smooth; model I.



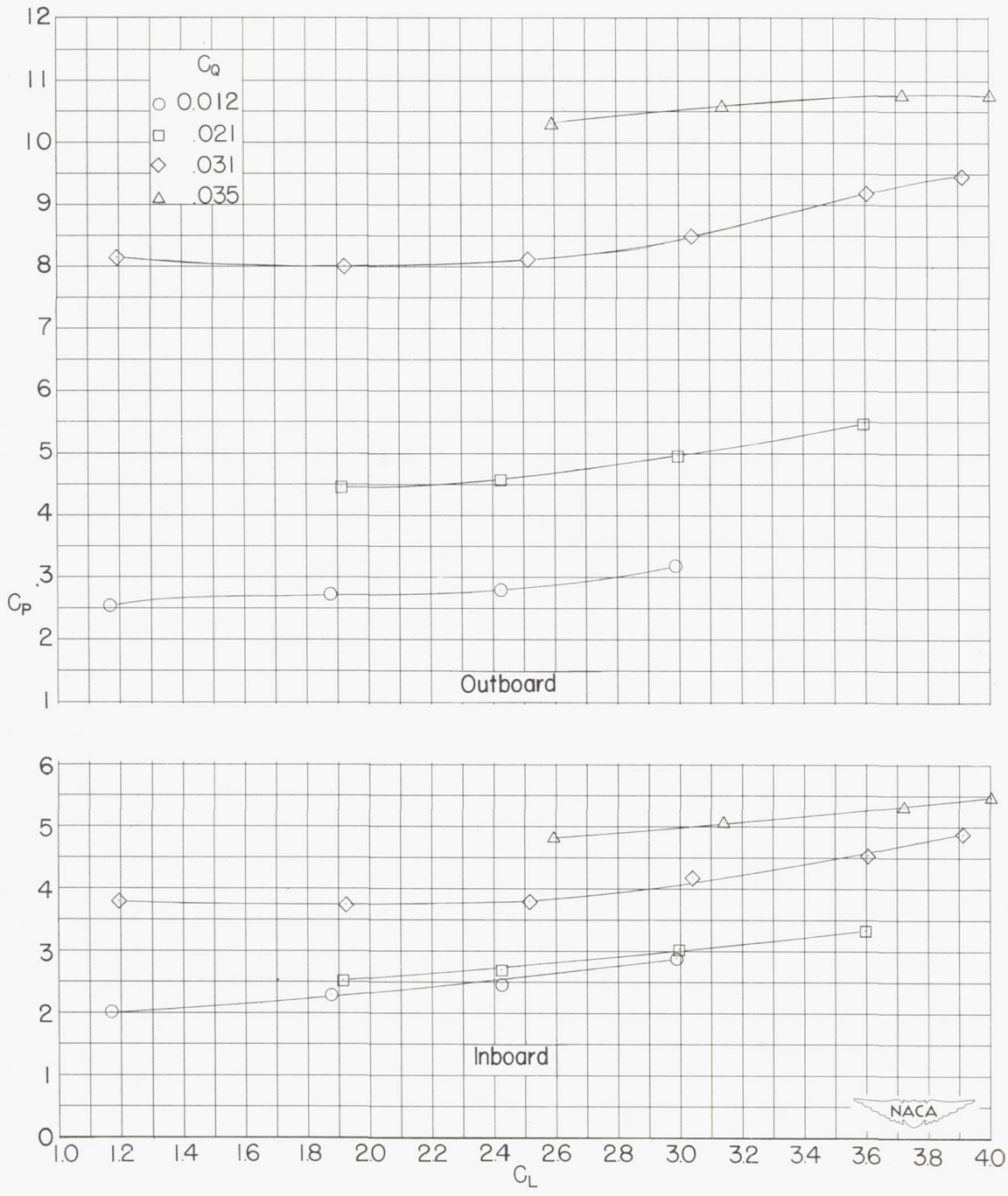
(b) Variation of pressure-loss coefficient with lift coefficient.

Figure 10.- Concluded.



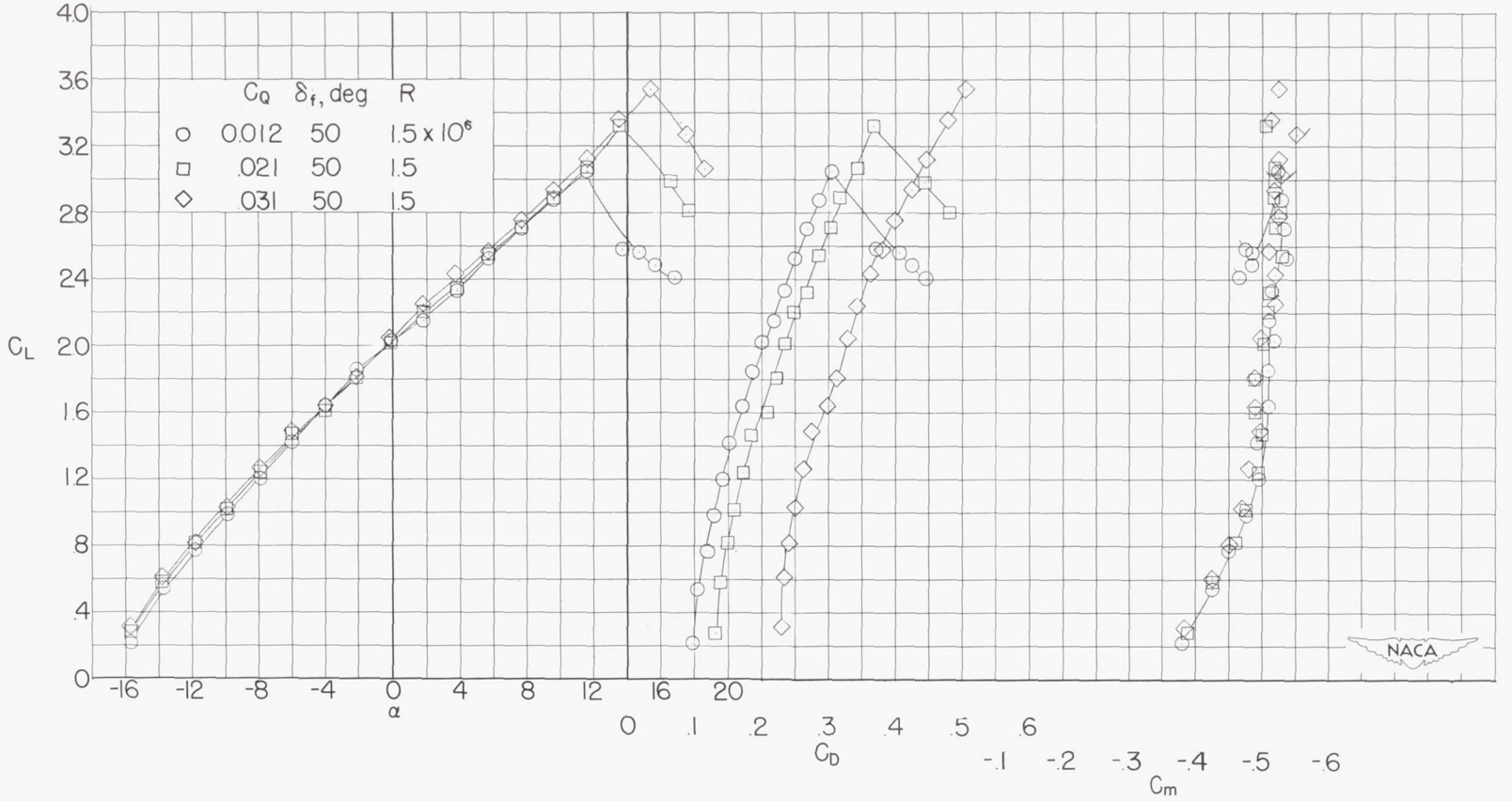
(a) Variation of C_L with α, C_D, and C_m.

Figure 11.- Aerodynamic characteristics of the wing with suction applied full span. Flaps deflected 45°; wing smooth; model I.



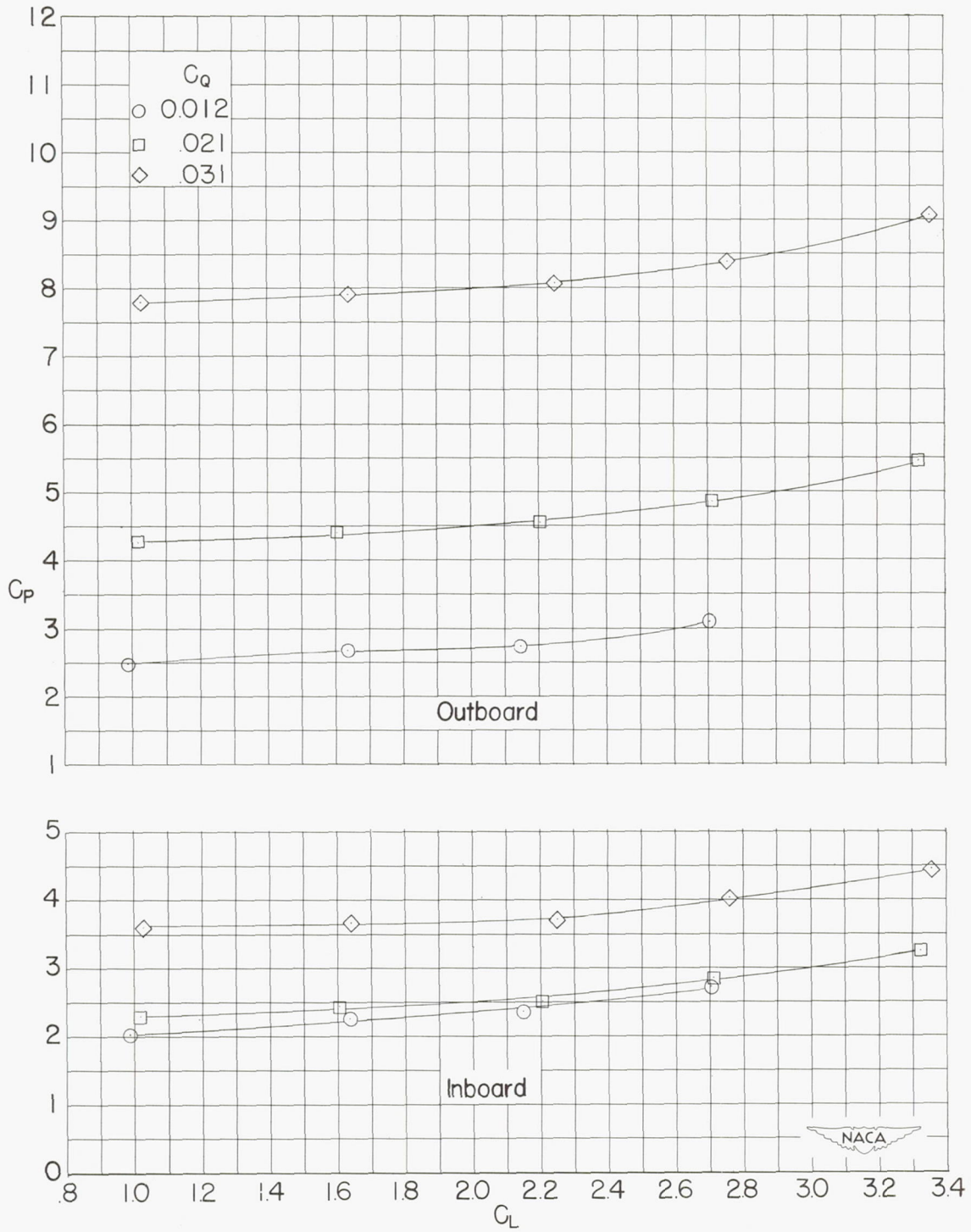
(b) Variation of pressure-loss coefficient with lift coefficient.

Figure 11.- Concluded.



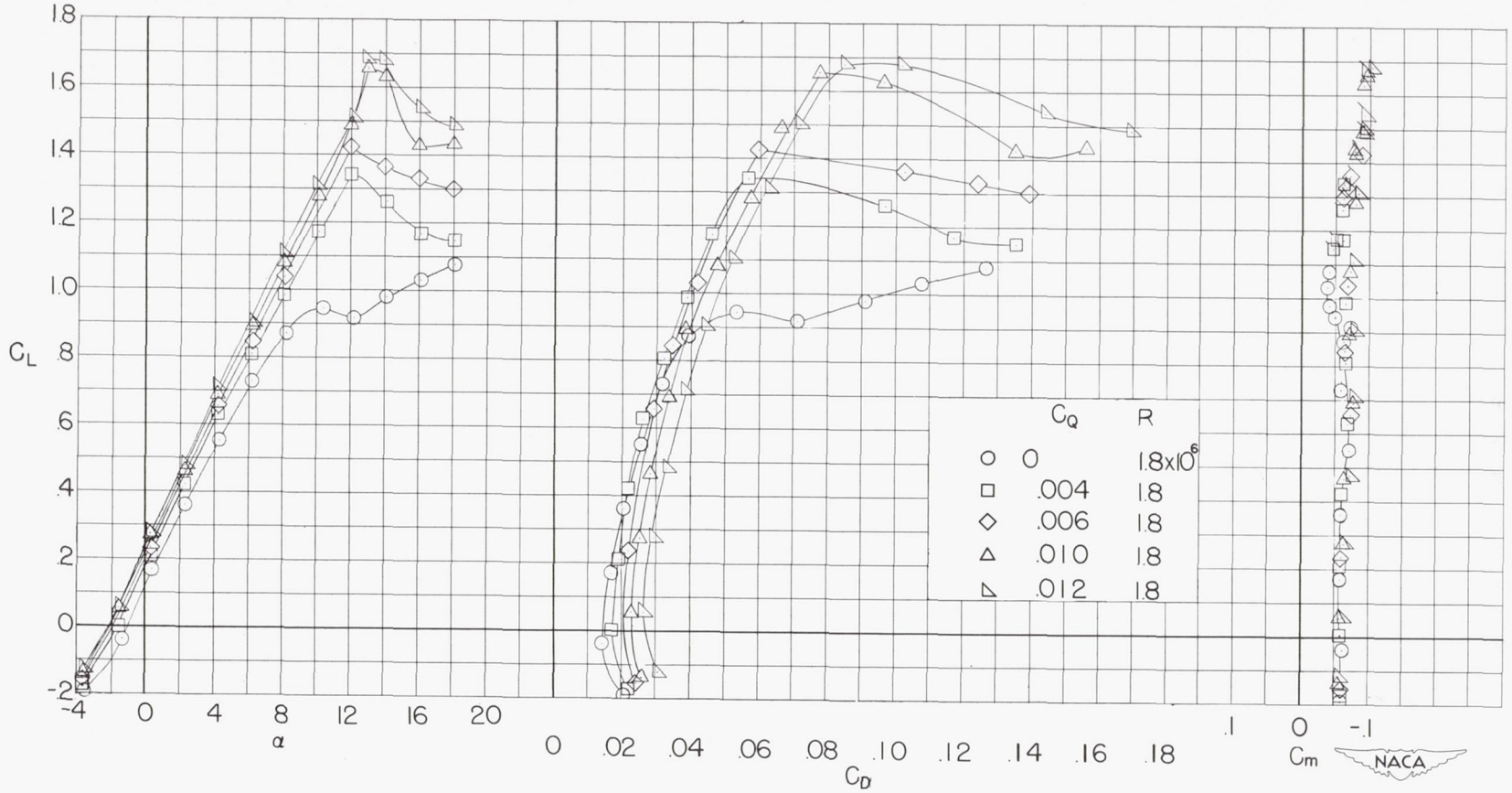
(a) Variation of C_L with α, C_D, and C_m.

Figure 12.- Aerodynamic characteristics of the wing with suction applied full span. Flaps deflected 50°; wing smooth; model I.



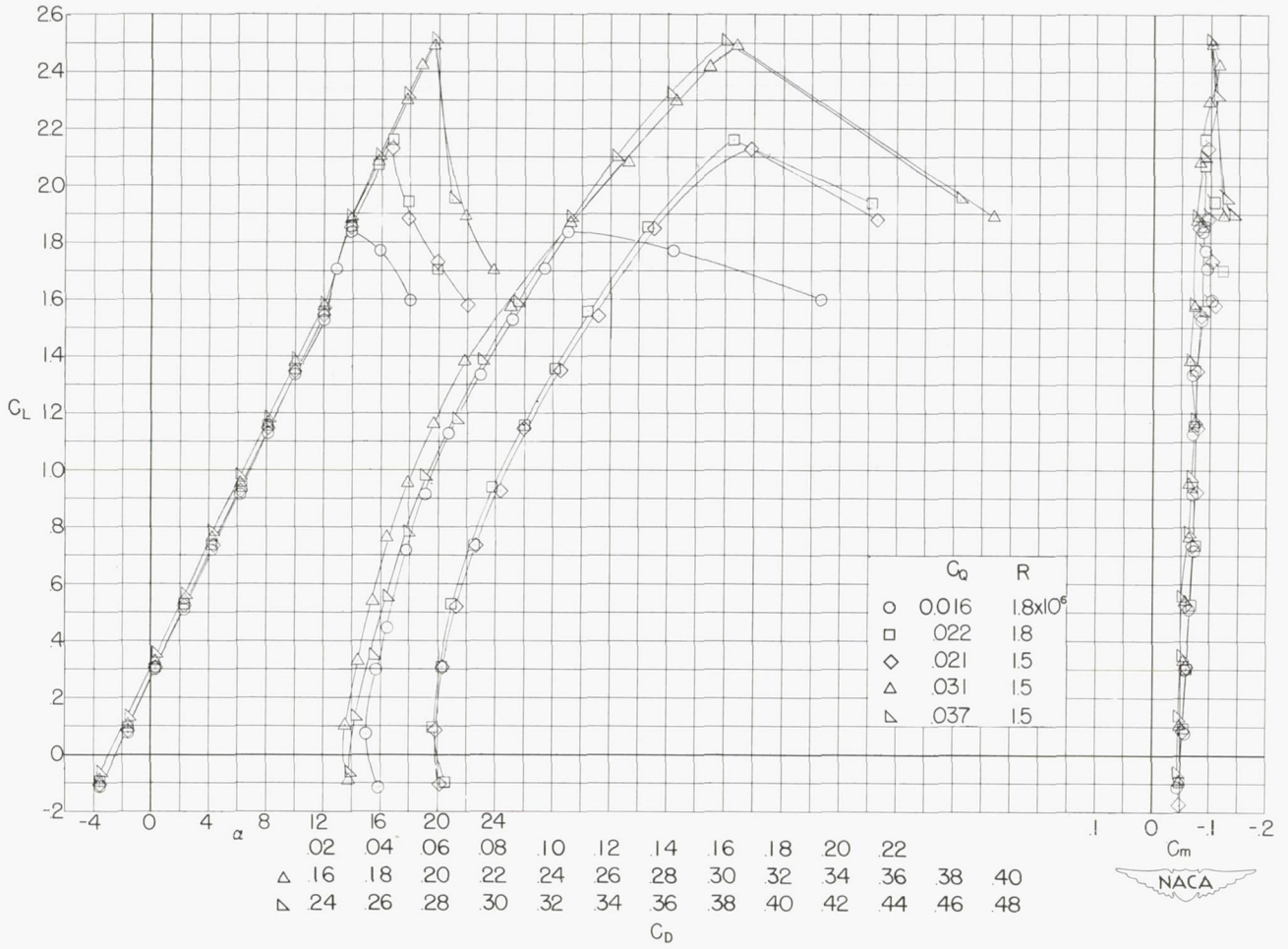
(b) Variation of pressure-loss coefficient with lift coefficient.

Figure 12.- Concluded.



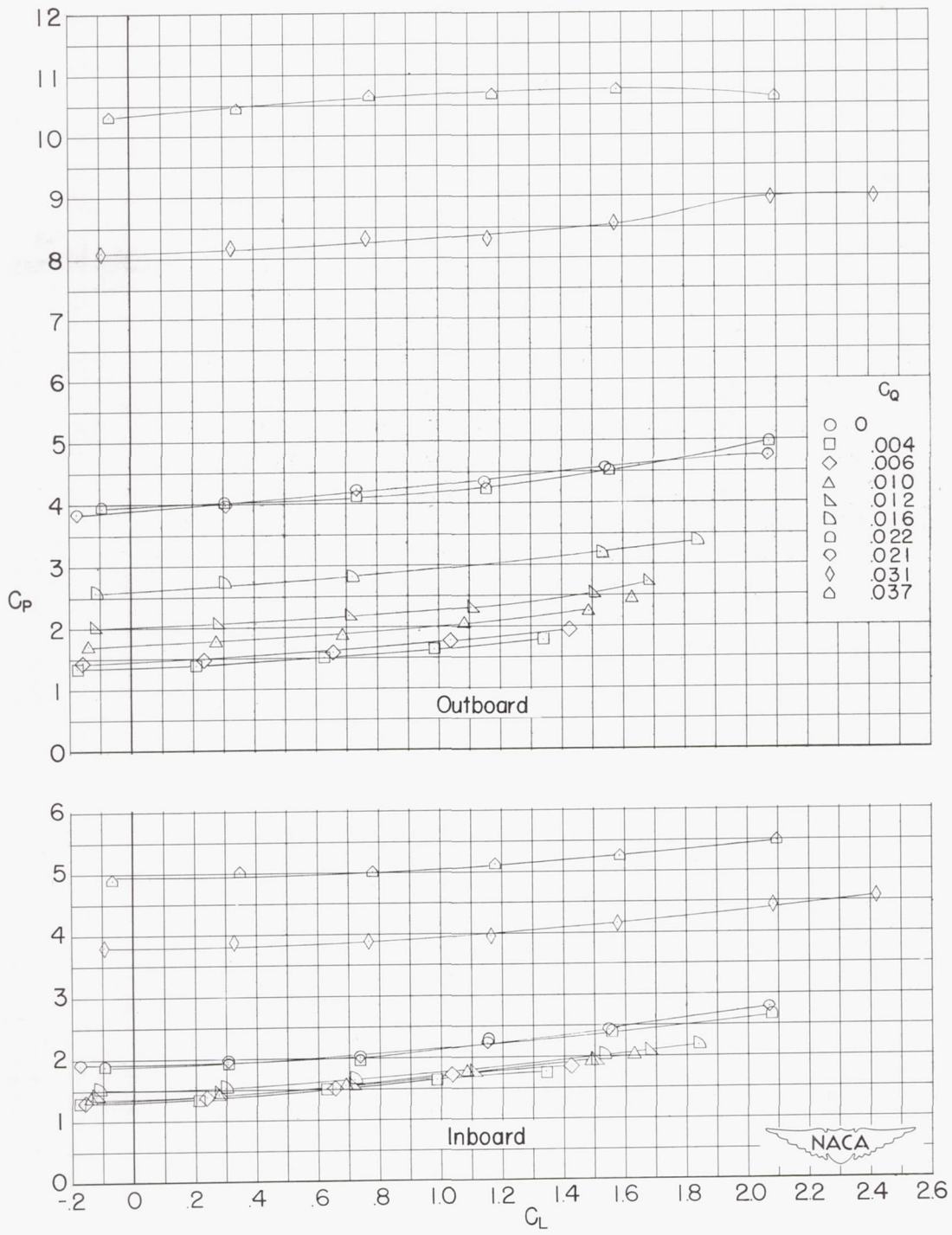
(a) Variation of C_L with α, C_D, and C_m.

Figure 13.- Aerodynamic characteristics of the wing with suction applied full span. Flaps removed; wing smooth; model I.



(a) Concluded. (Note that C_D values for C_Q above 0.021 are plotted on different scales.)

Figure 13.- Continued.



(b) Variation of pressure-loss coefficient with lift coefficient.

Figure 13.- Concluded.

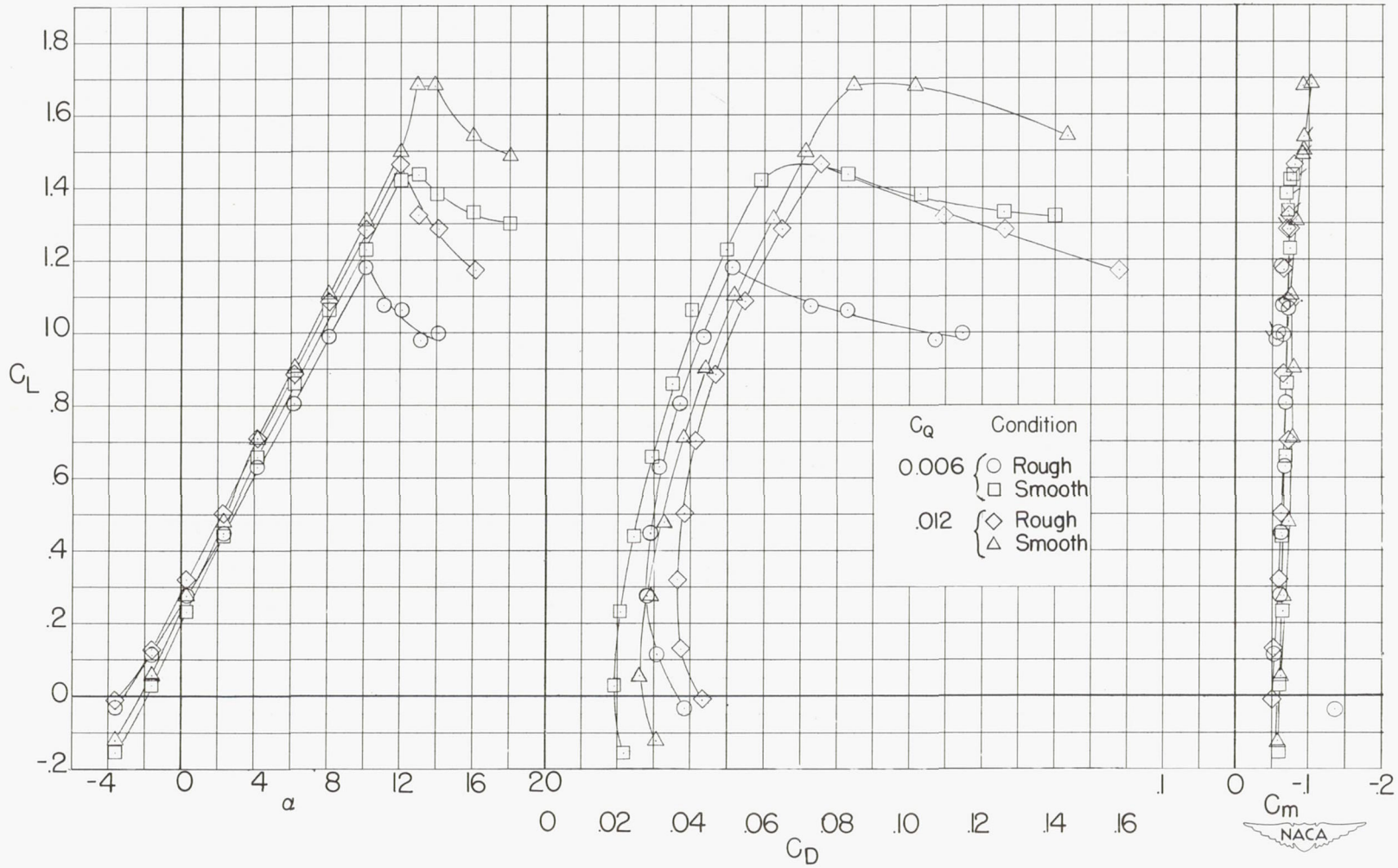


Figure 14.- A comparison of the wing smooth and the wing with leading-edge roughness. Suction applied full span; flaps removed; model I.

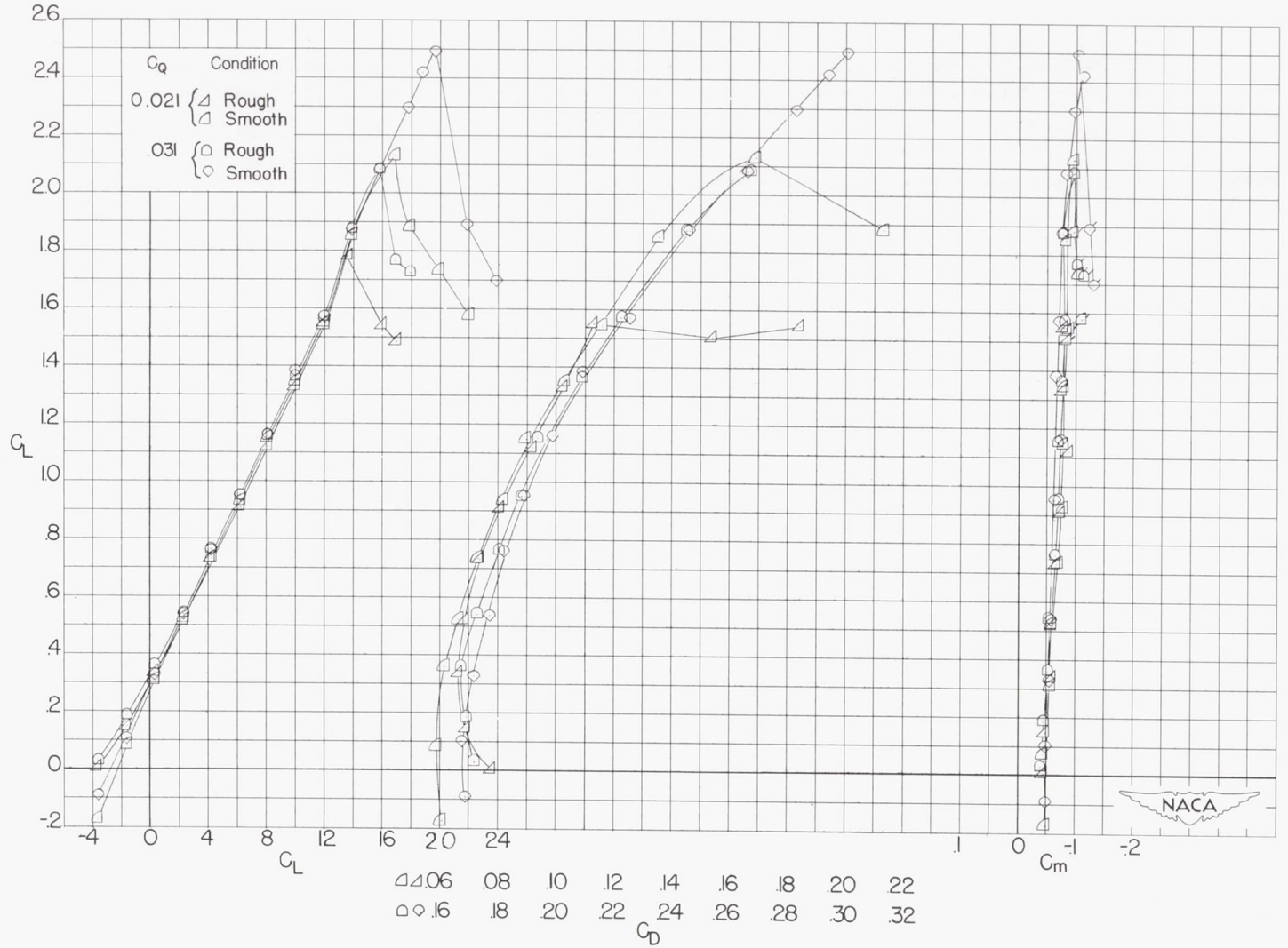


Figure 14.- Concluded. (Note that C_D values are plotted on different scales.)

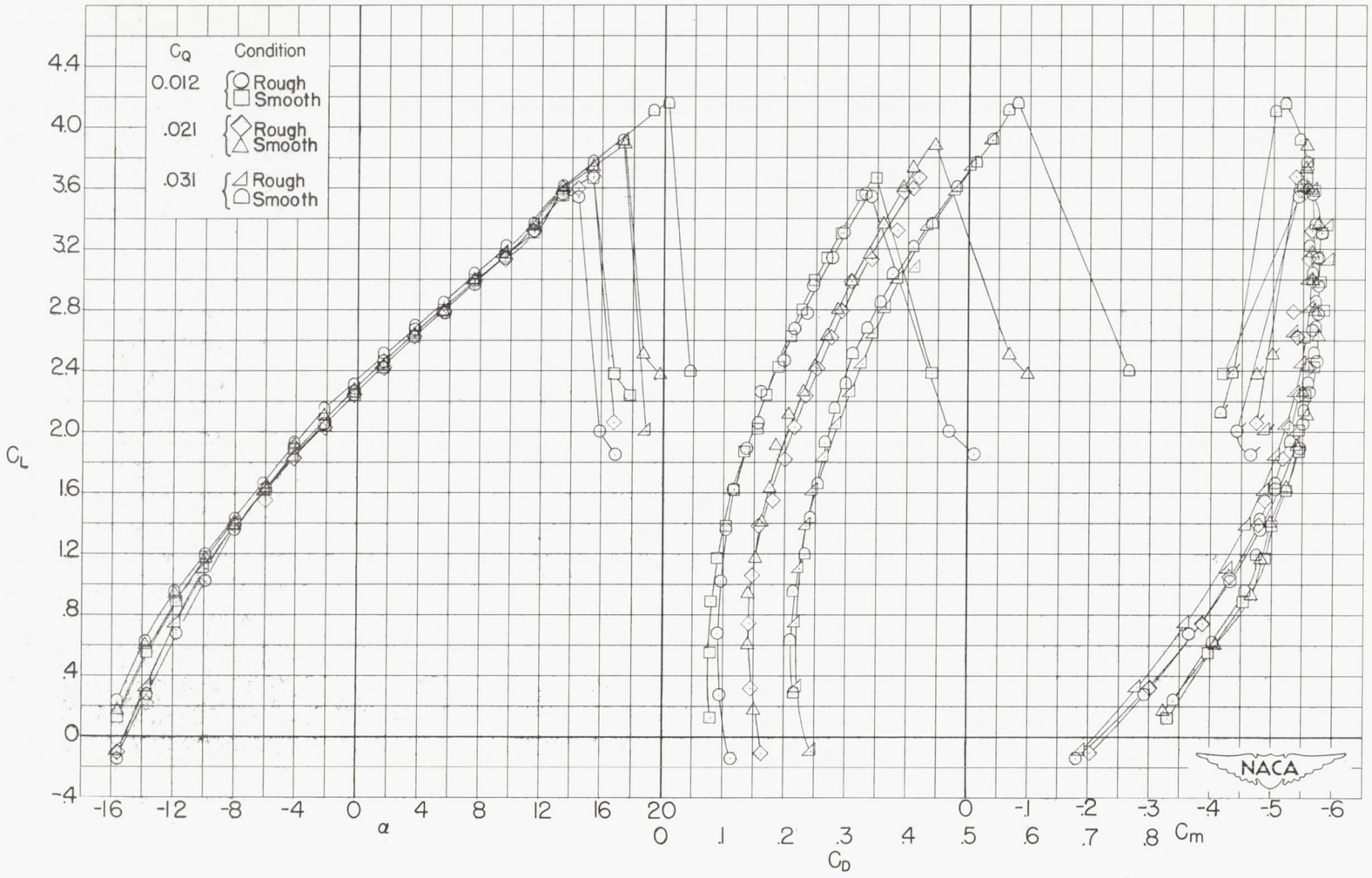


Figure 15.- A comparison of aerodynamic characteristics with the wing smooth and the wing with leading-edge roughness. Suction applied full span; flaps deflected 45°; R = 1.5×10^6; model I.

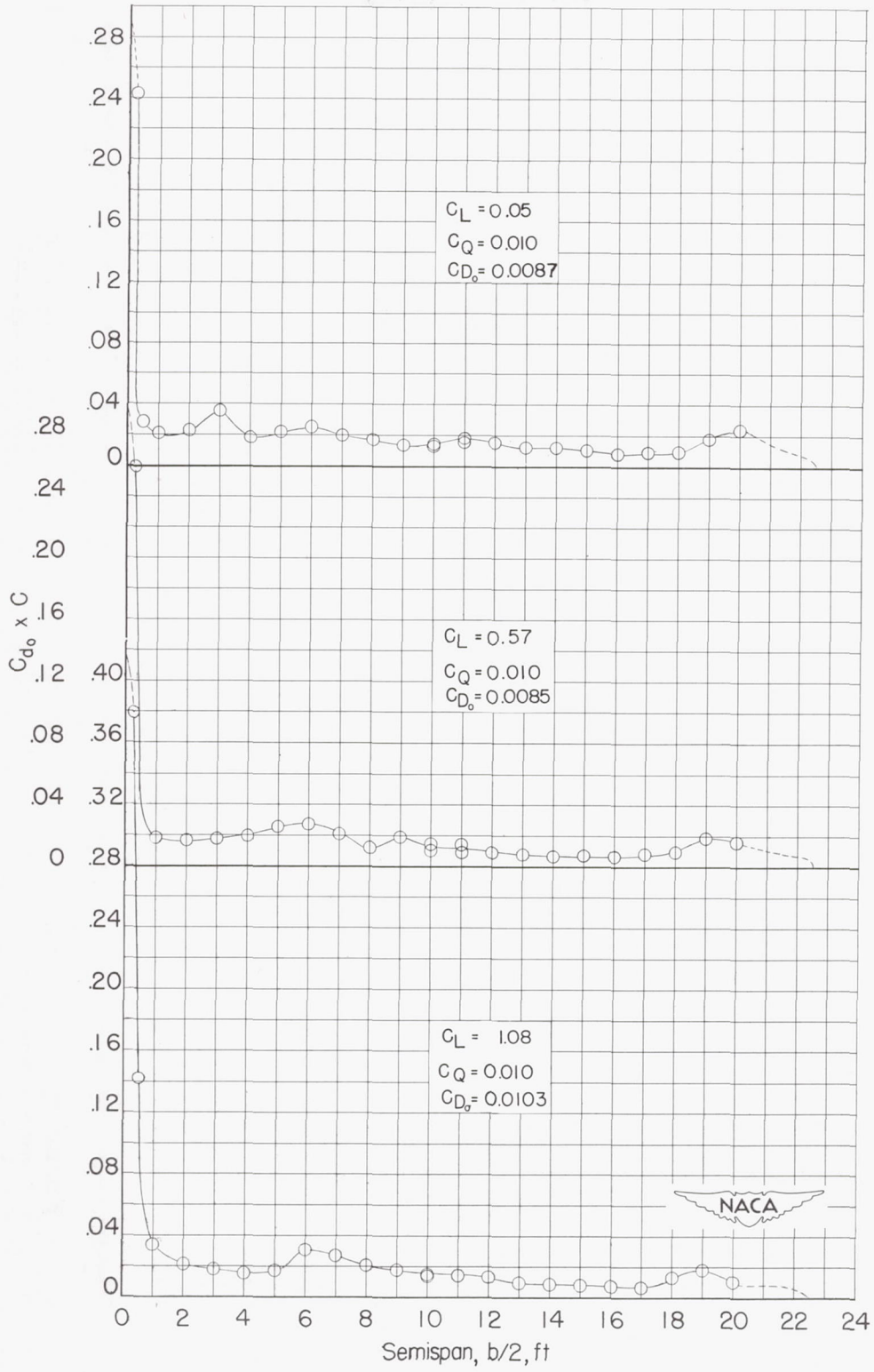


Figure 16.- Distribution of profile drag across the semispan at several lift coefficients. Full-span suction; flaps removed; model I.

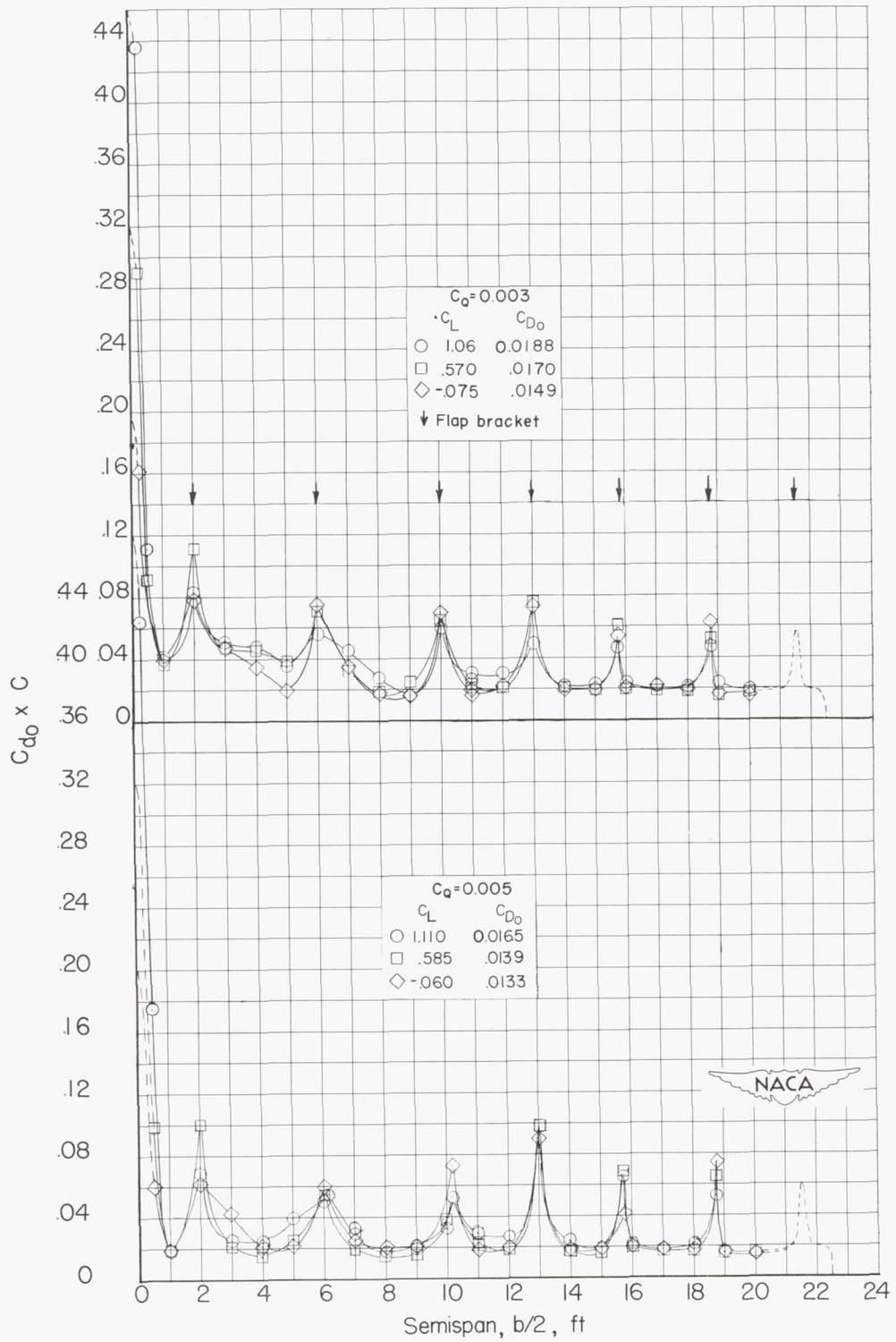


Figure 17.- Distribution of profile drag across the span at several lift coefficients. Suction only on 2 to 0 percent chord tapered semispan slot; flaps installed; model I.

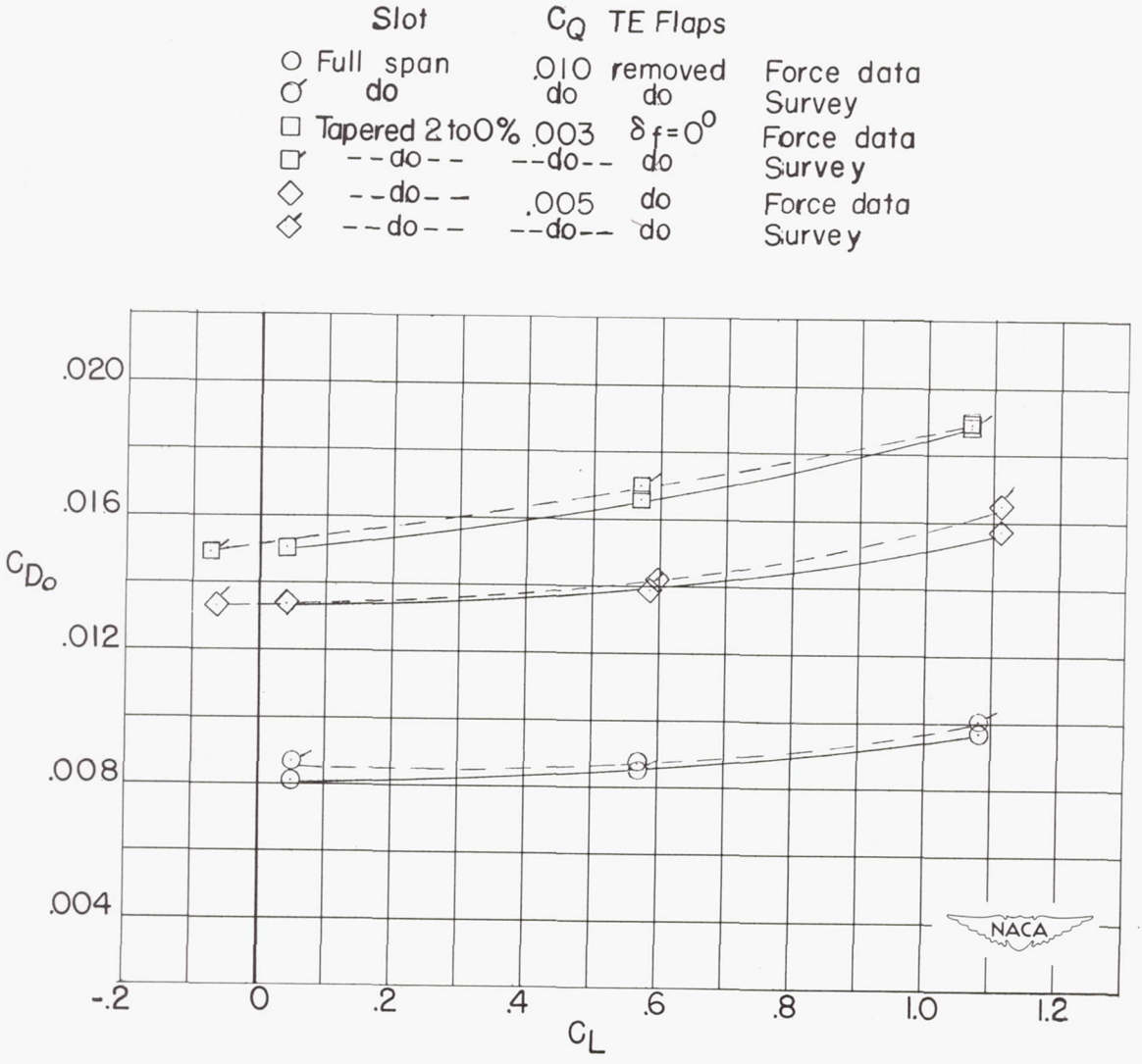
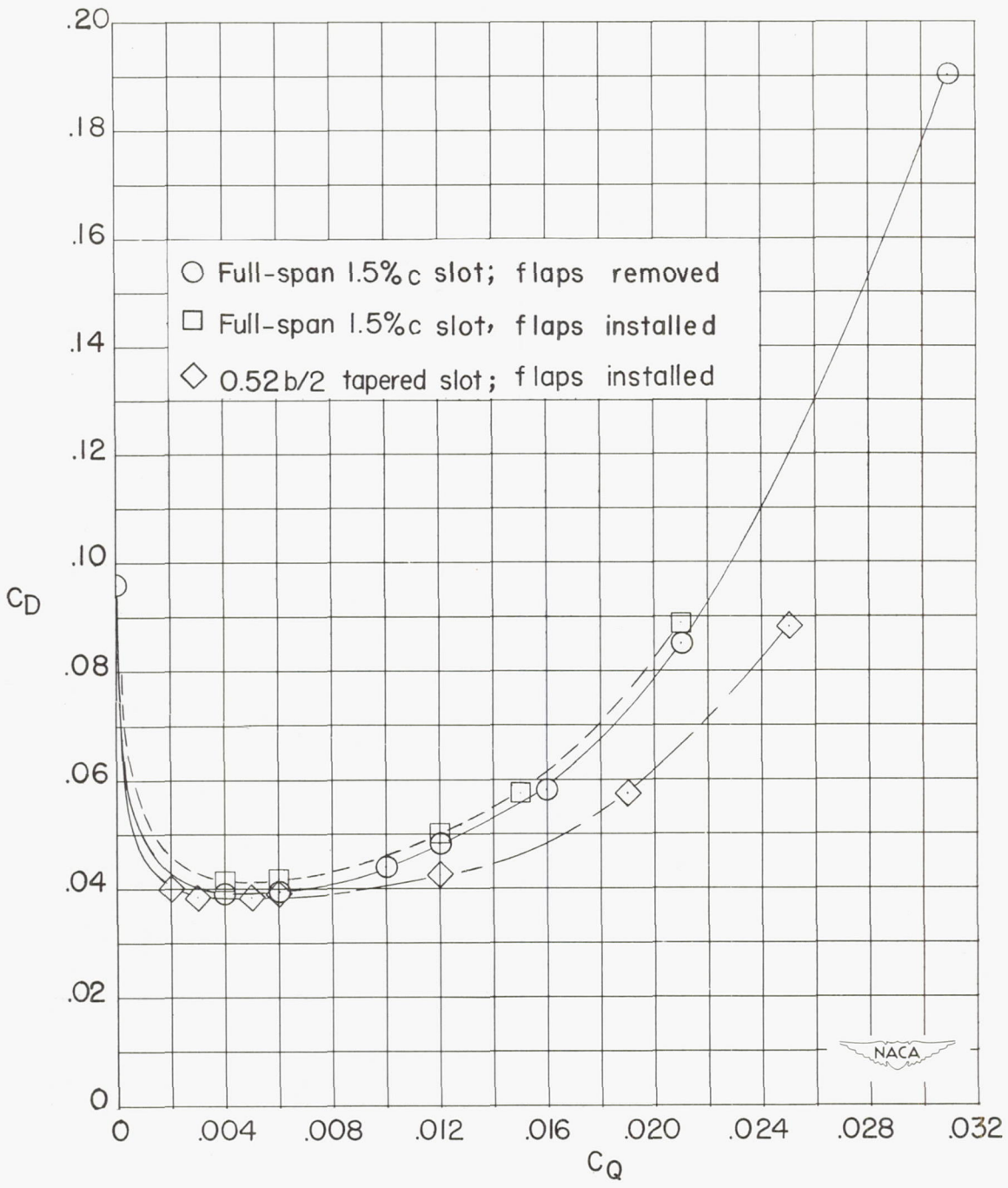
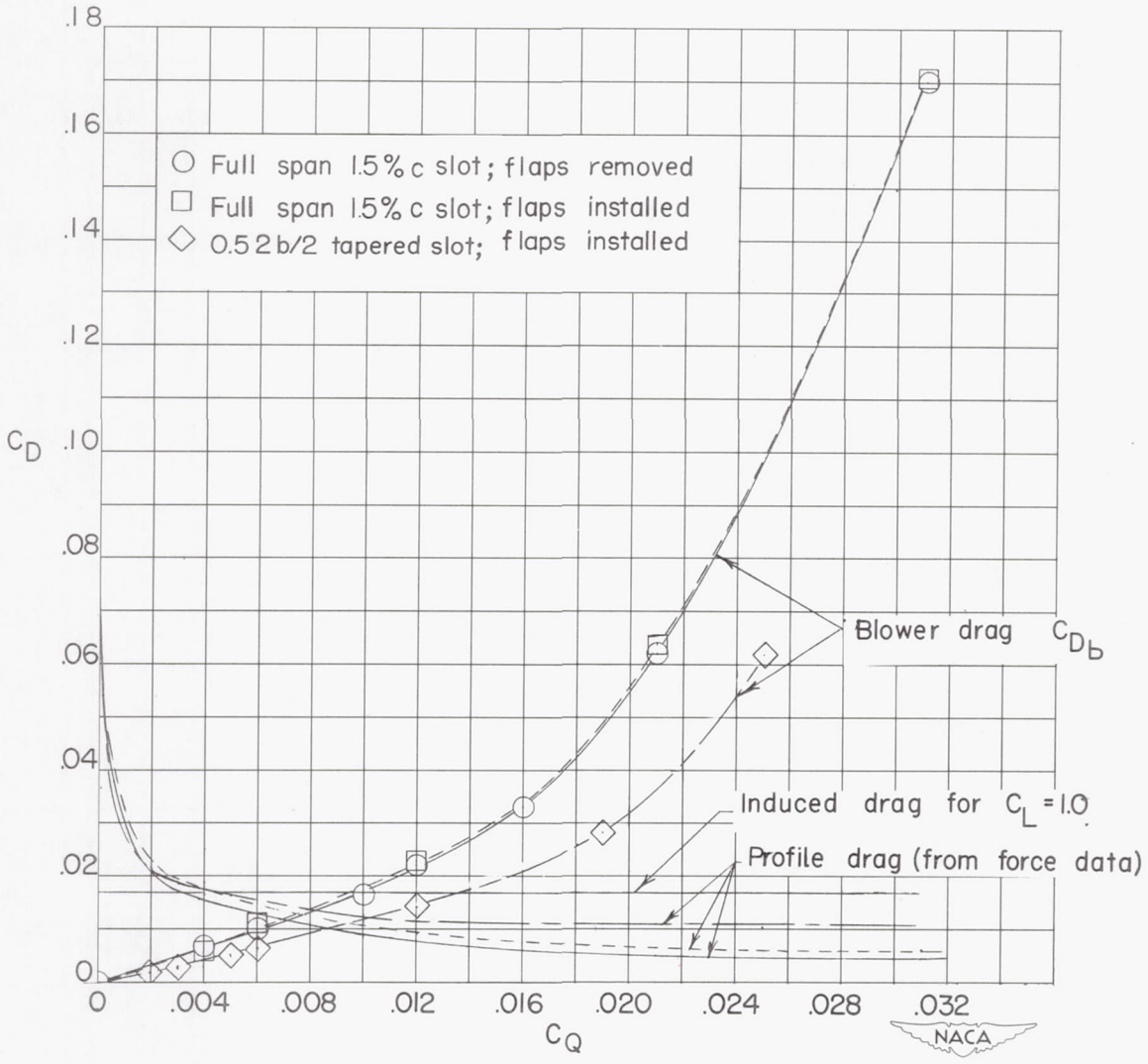


Figure 18.- Comparison of profile drag for model I as determined from force tests and wake surveys.



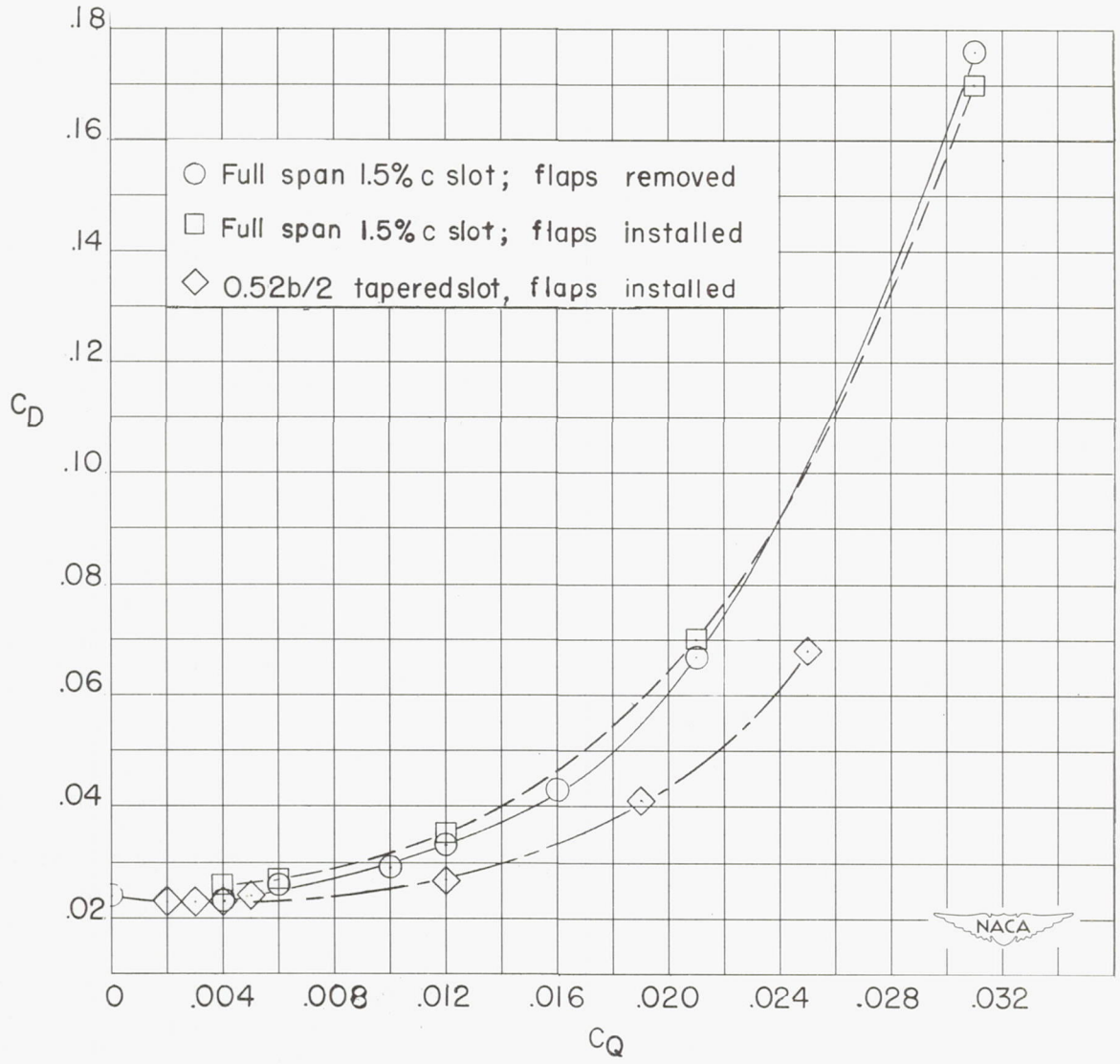
(a) Wing total drag.

Figure 19.- Variation of total drag, profile drag, and blower drag with suction-flow quantity. Wing smooth; $R = 1.8 \times 10^6$; $C_L = 1.0$; model I.



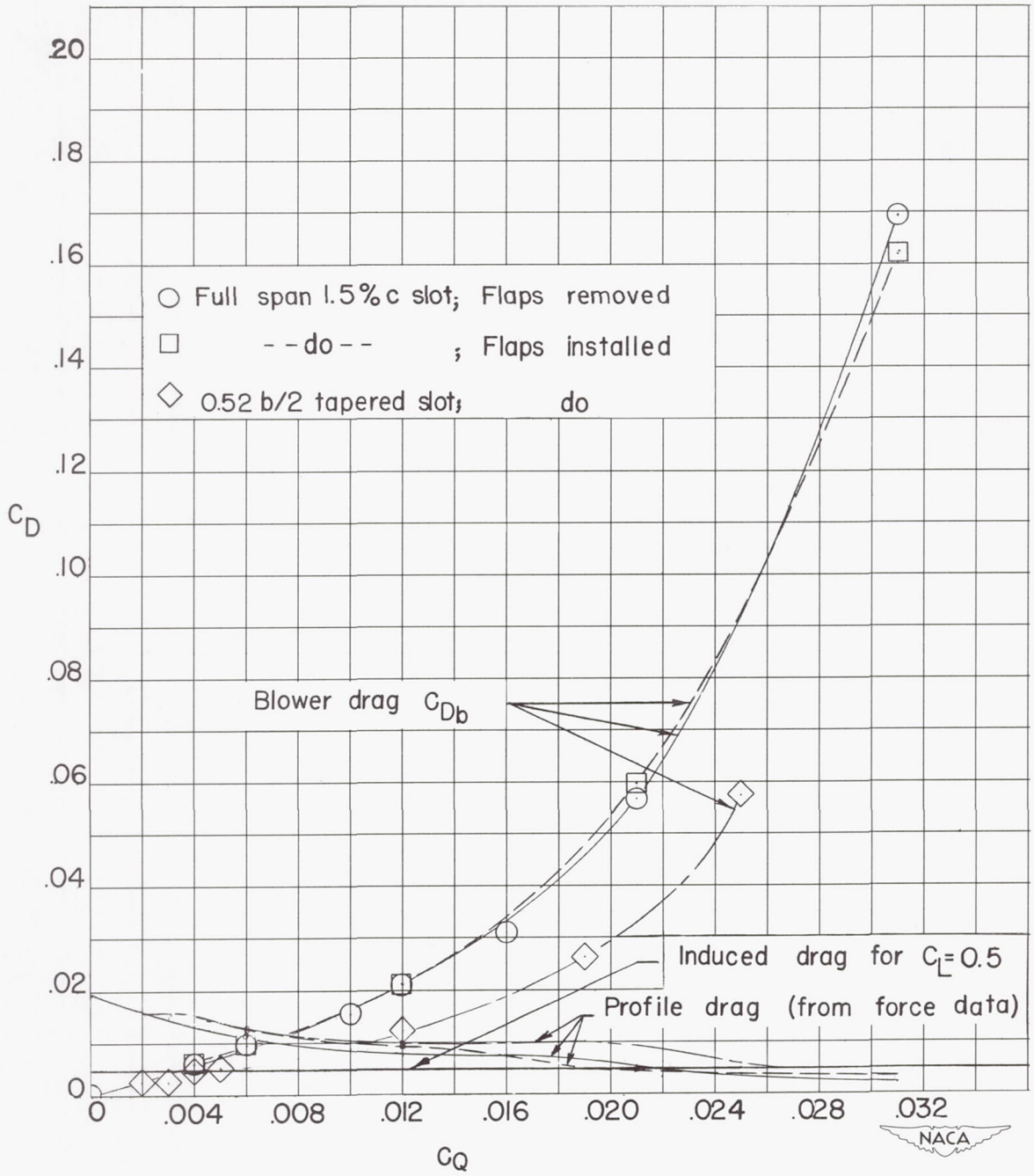
(b) Profile and blower drag.

Figure 19.- Concluded.



(a) Wing total drag.

Figure 20.- Variation of total drag, profile drag, and blower drag with suction-flow quantity. Wing smooth; C_L = 0.5; model I.



(b) Profile and blower drag.

Figure 20.- Concluded.

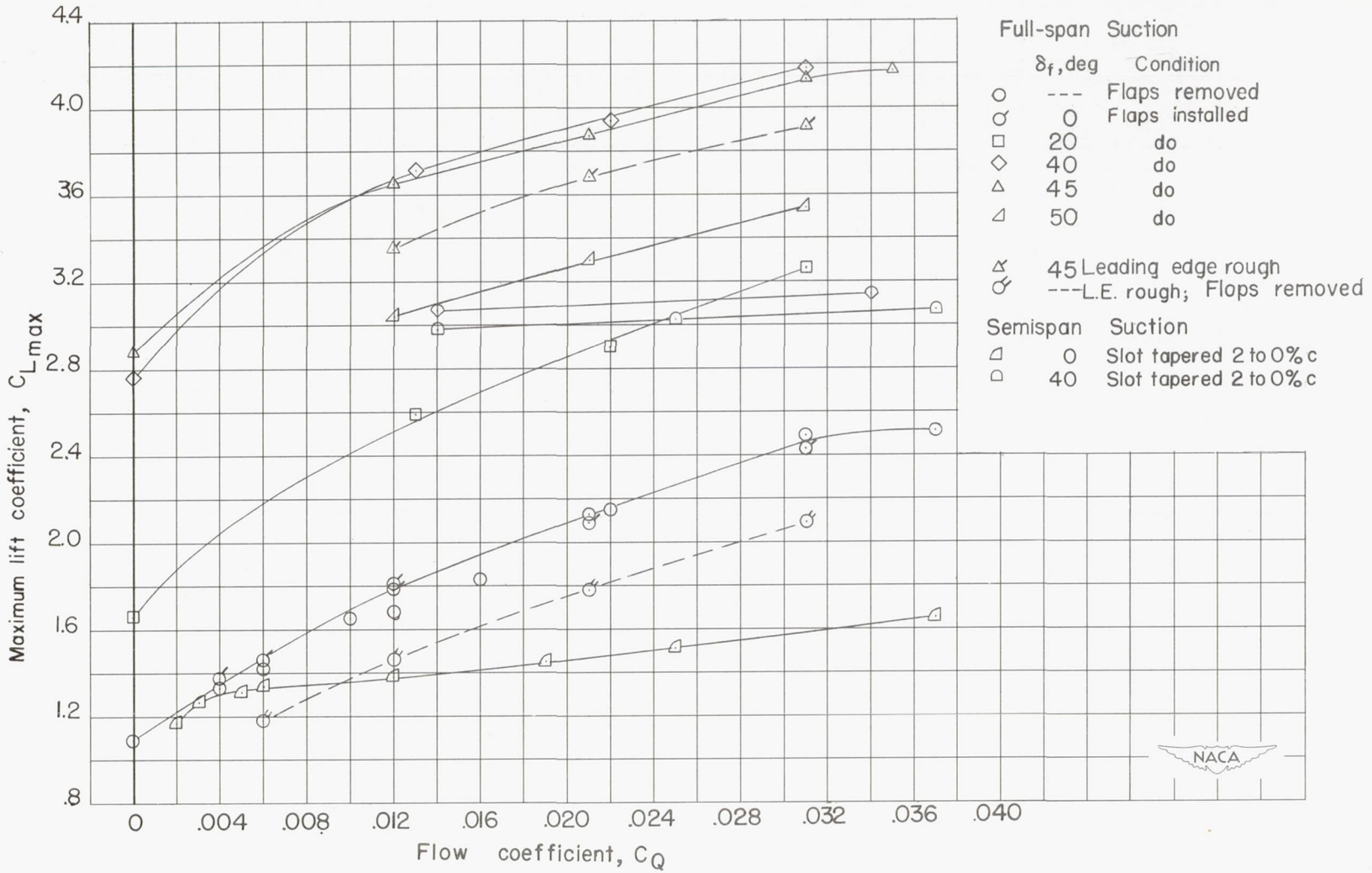


Figure 21.- Effect of suction, flap deflection, and leading-edge roughness on the maximum lift characteristics of model I.

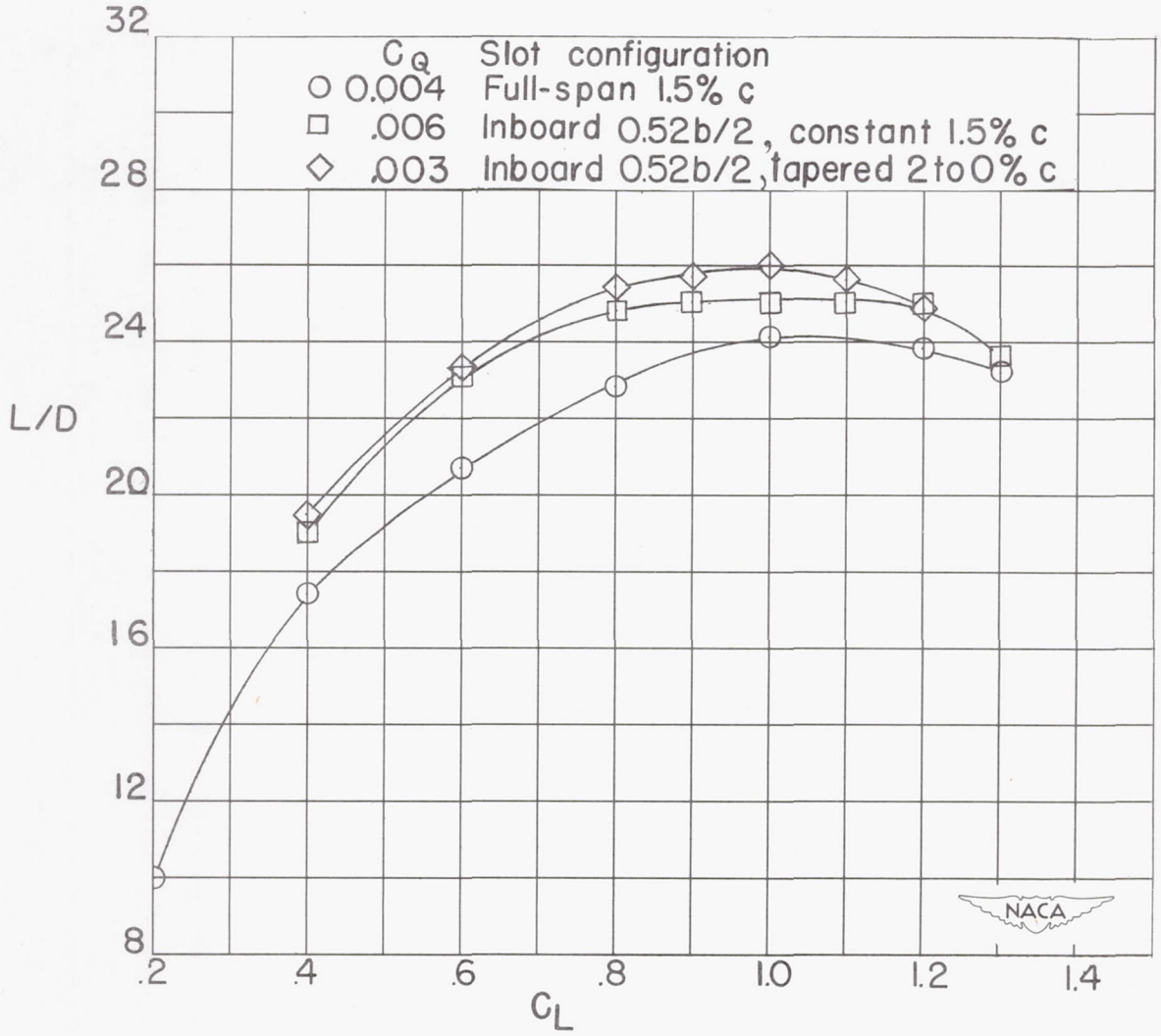


Figure 22.- Variation of lift-drag ratio with lift coefficient for three slot configurations. $\delta_f = 0^o$; $R = 1.8 \times 10^6$; model I.

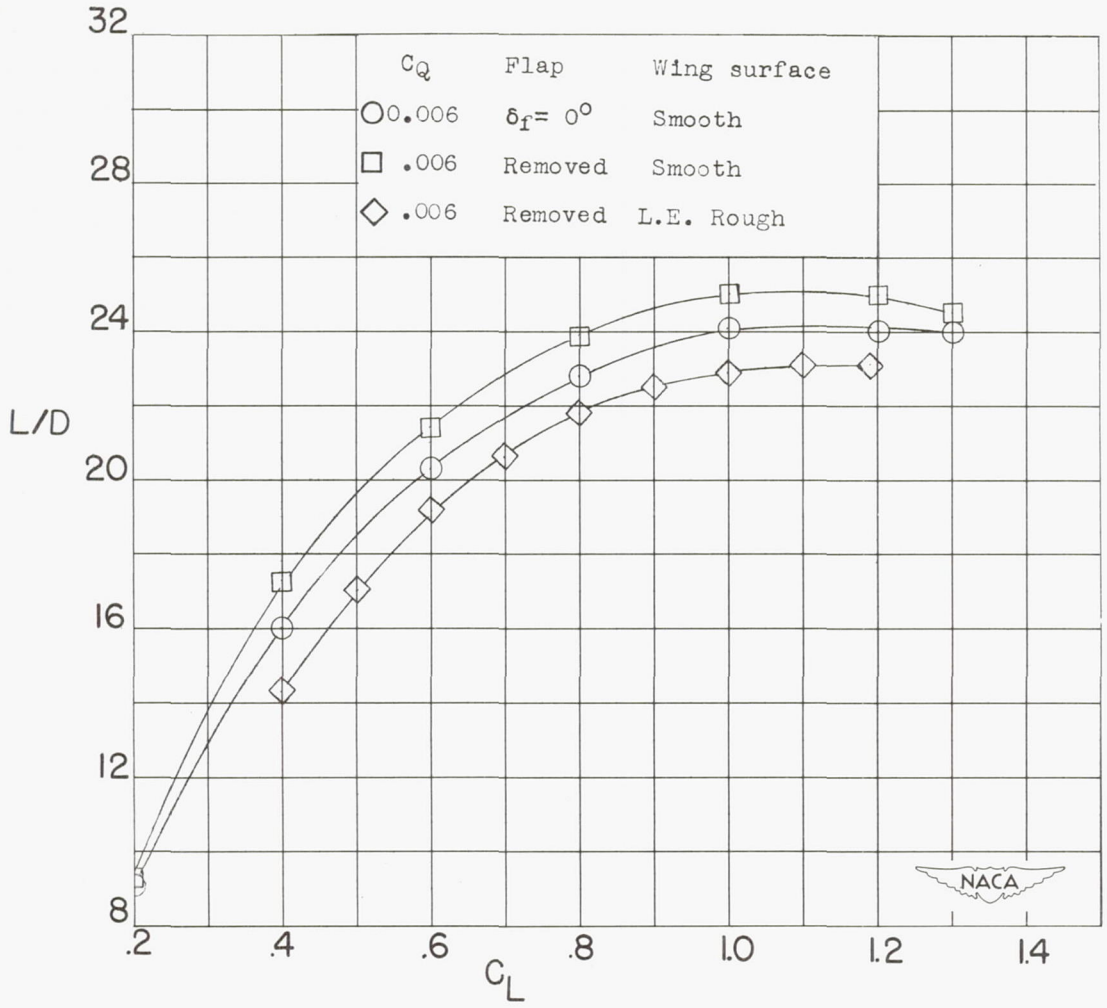


Figure 23.- Effect of flap installation and leading-edge roughness on the lift-drag ratio with full-span 1.5-percent-chord suction slot. $R = 1.8 \times 10^6$; model I.

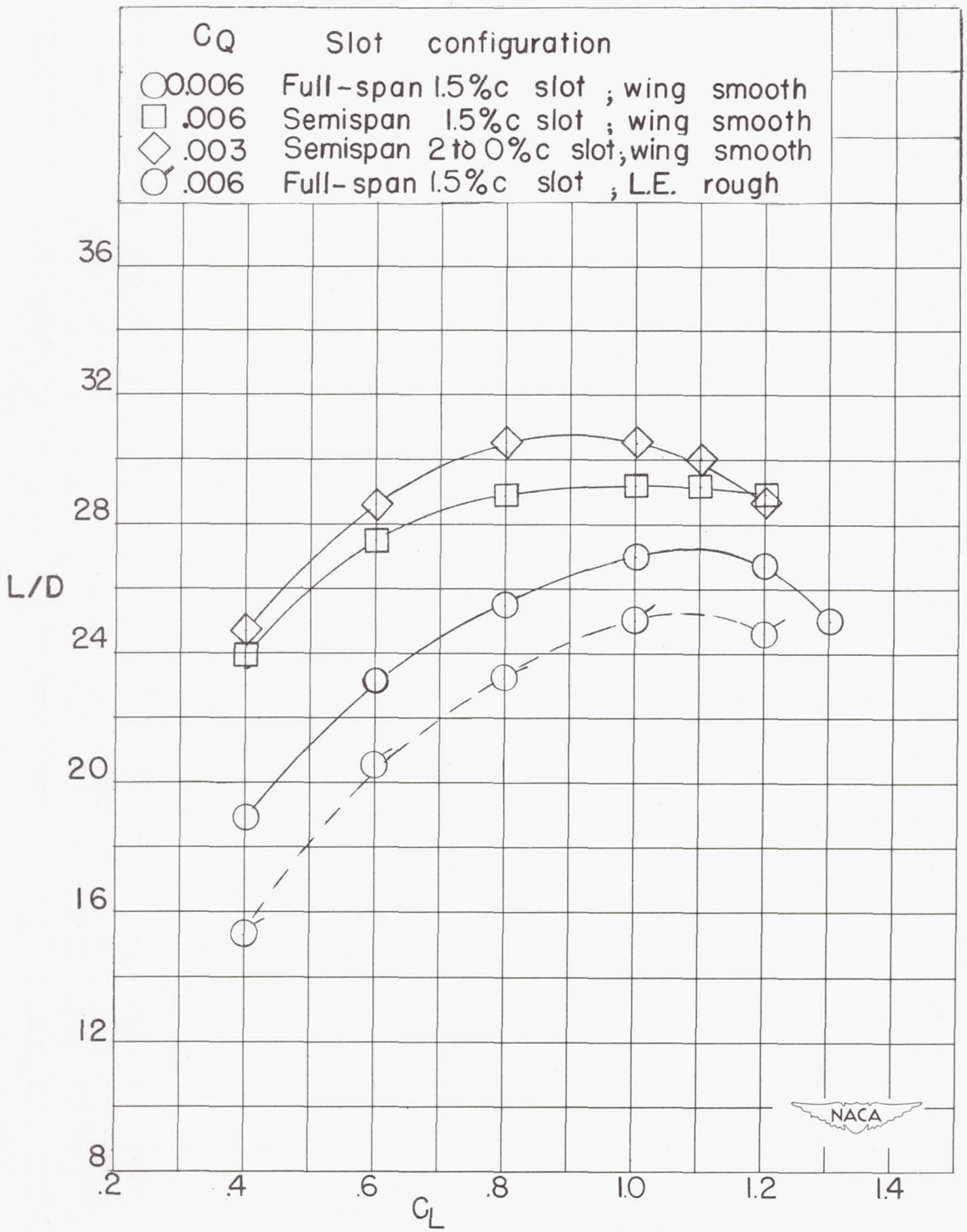


Figure 24.- Comparison of lift-drag-ratio characteristics of model I corrected for reflection-plane interference.

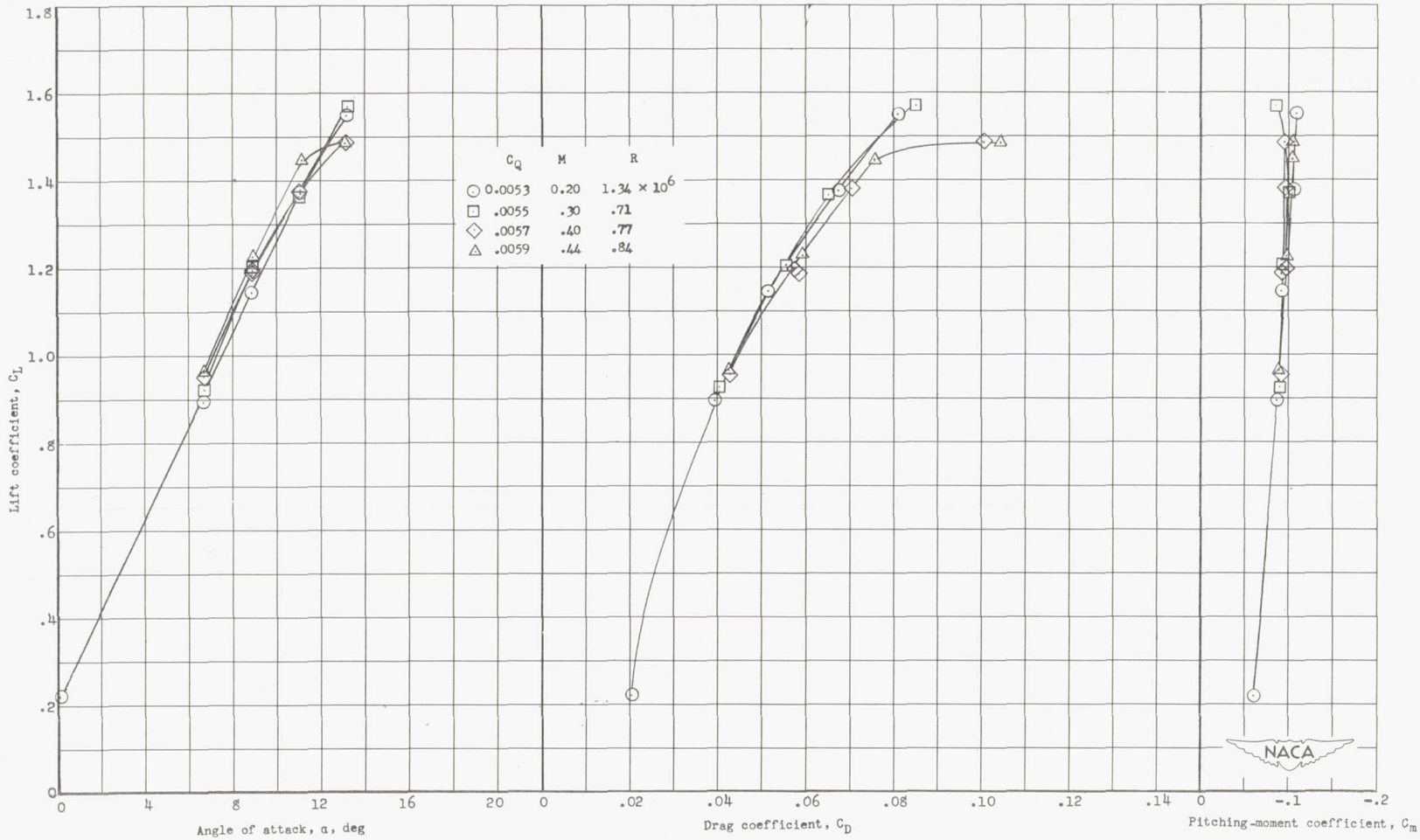


Figure 25.- Effect of Mach number on the aerodynamic characteristics of model II with boundary-layer control by suction. Model smooth.

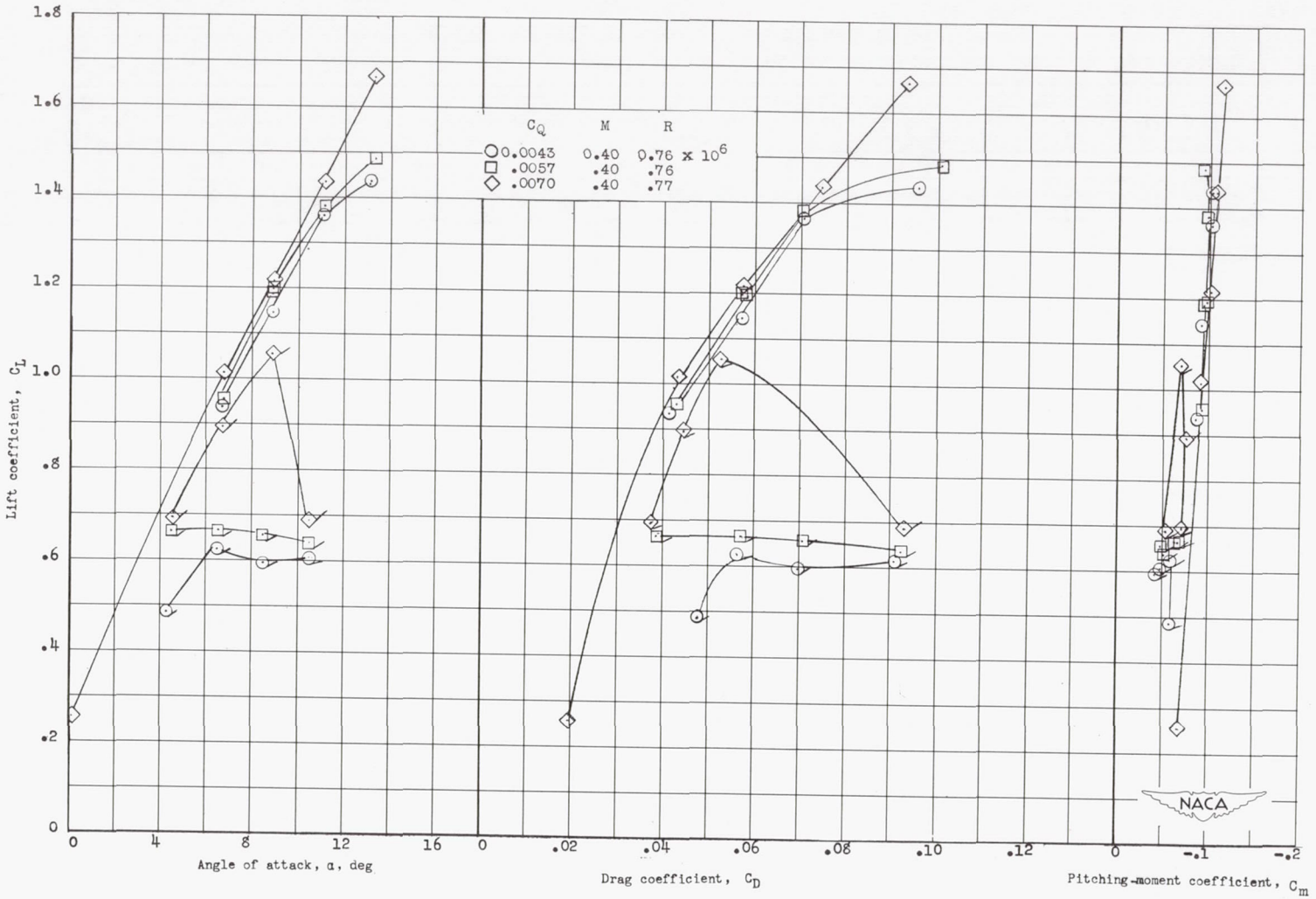
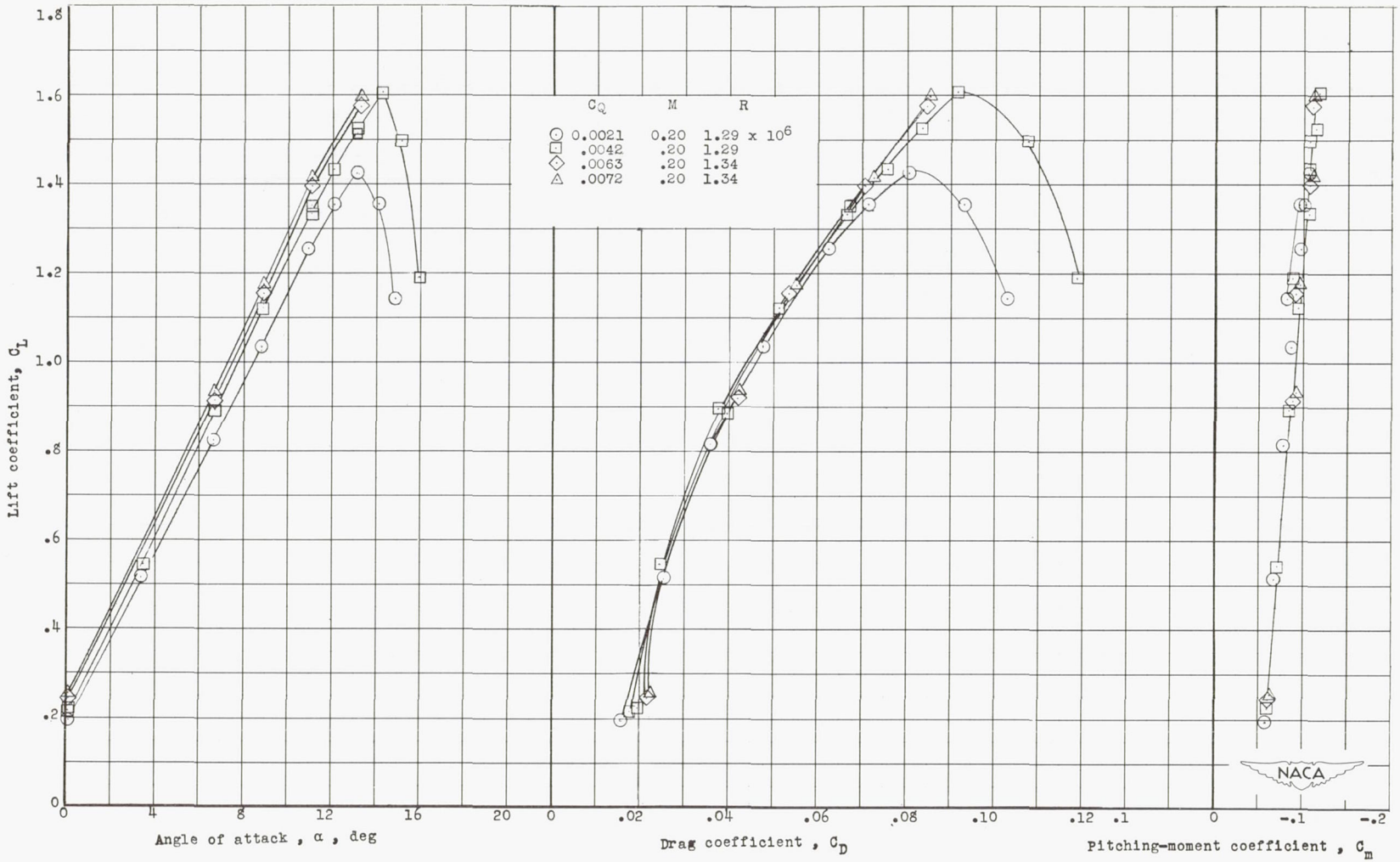
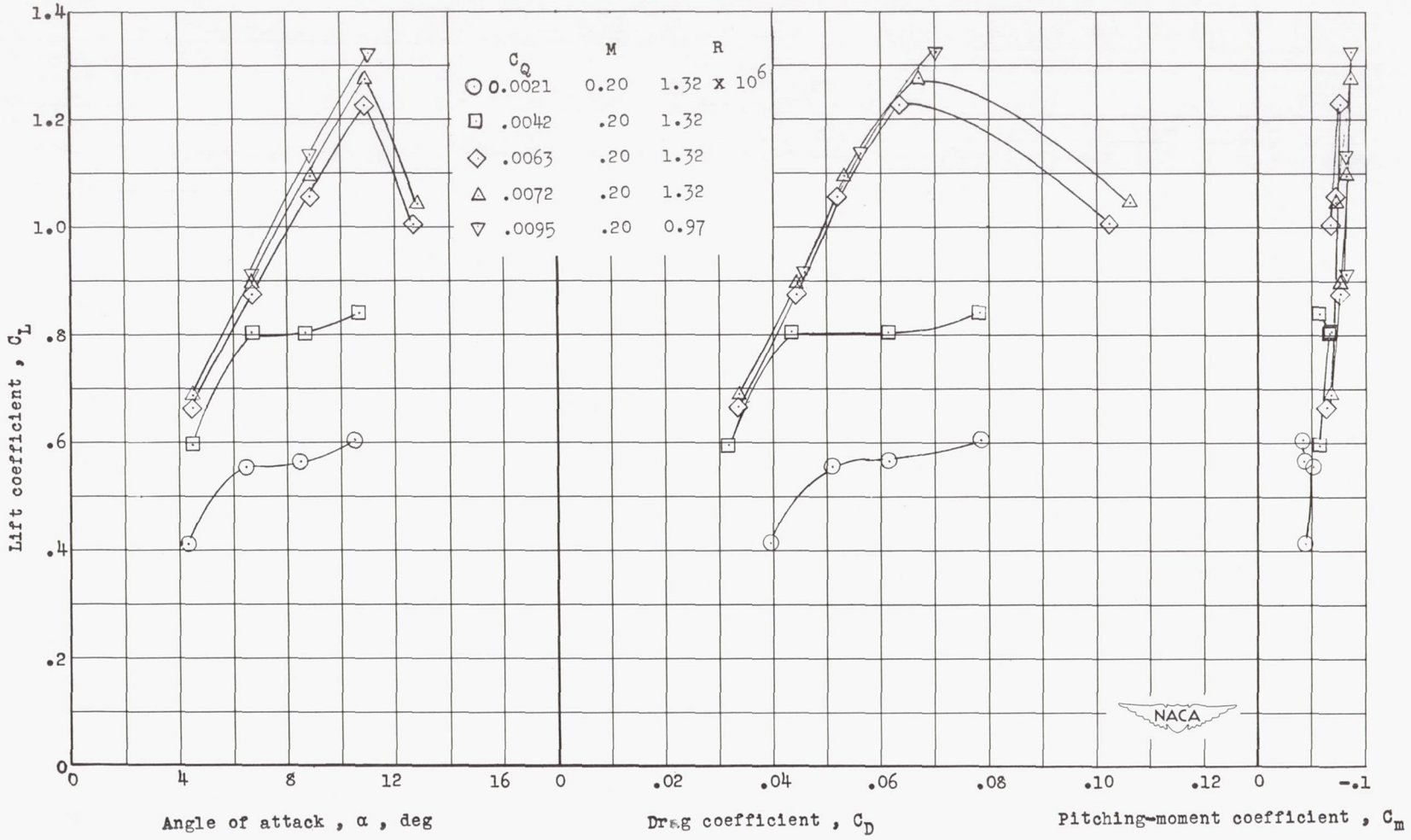


Figure 26.- Effect of boundary-layer control by suction on the aerodynamic characteristics of an unswept semispan wing with and without roughness. Model II. Flagged symbols denote roughness strips.



(a) Wing smooth; model II.

Figure 27.- Effect of boundary-layer control by suction on the aerodynamic characteristics of an unswept semispan wing.



(b) Wing rough; model II.

Figure 27.- Concluded.

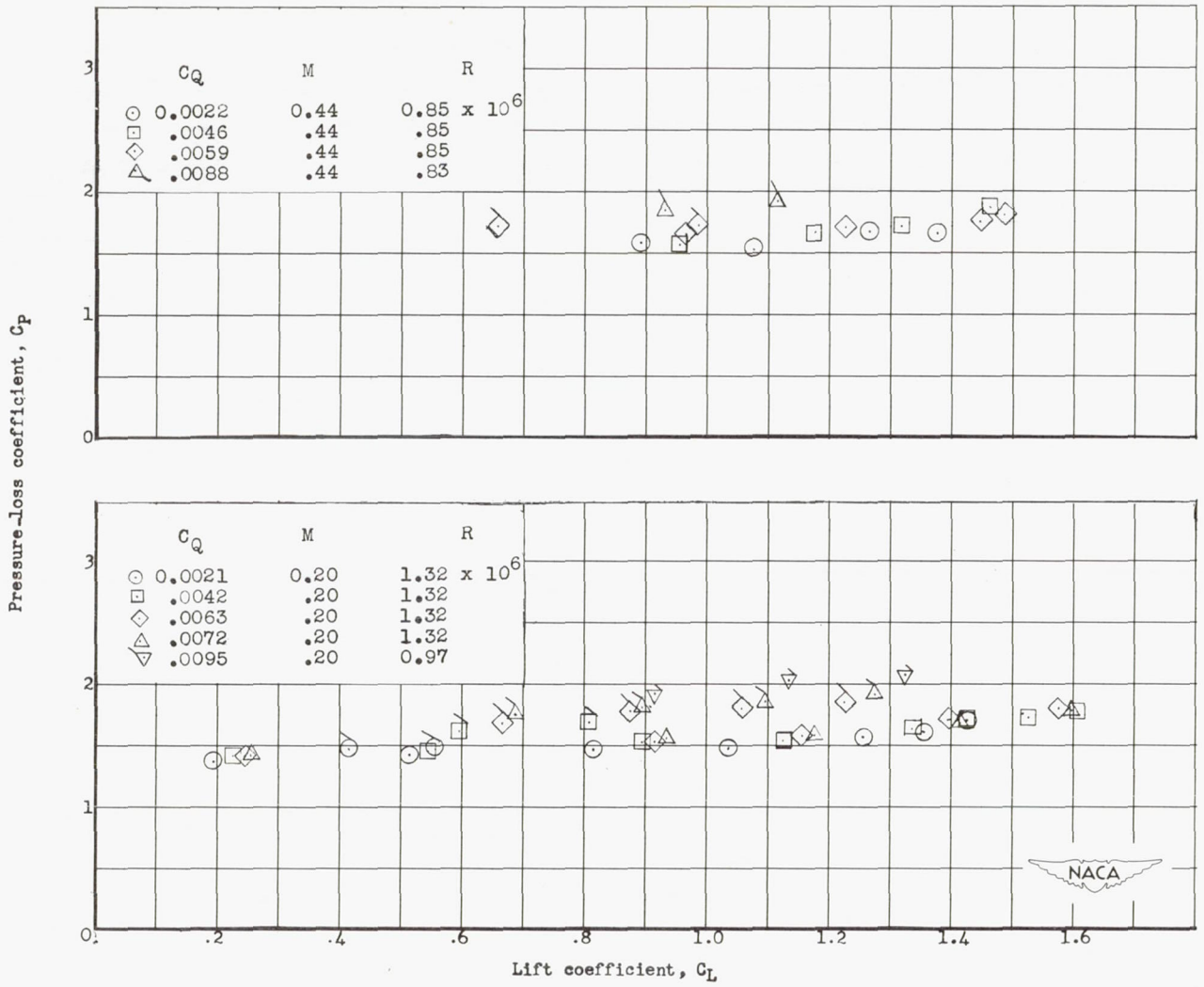
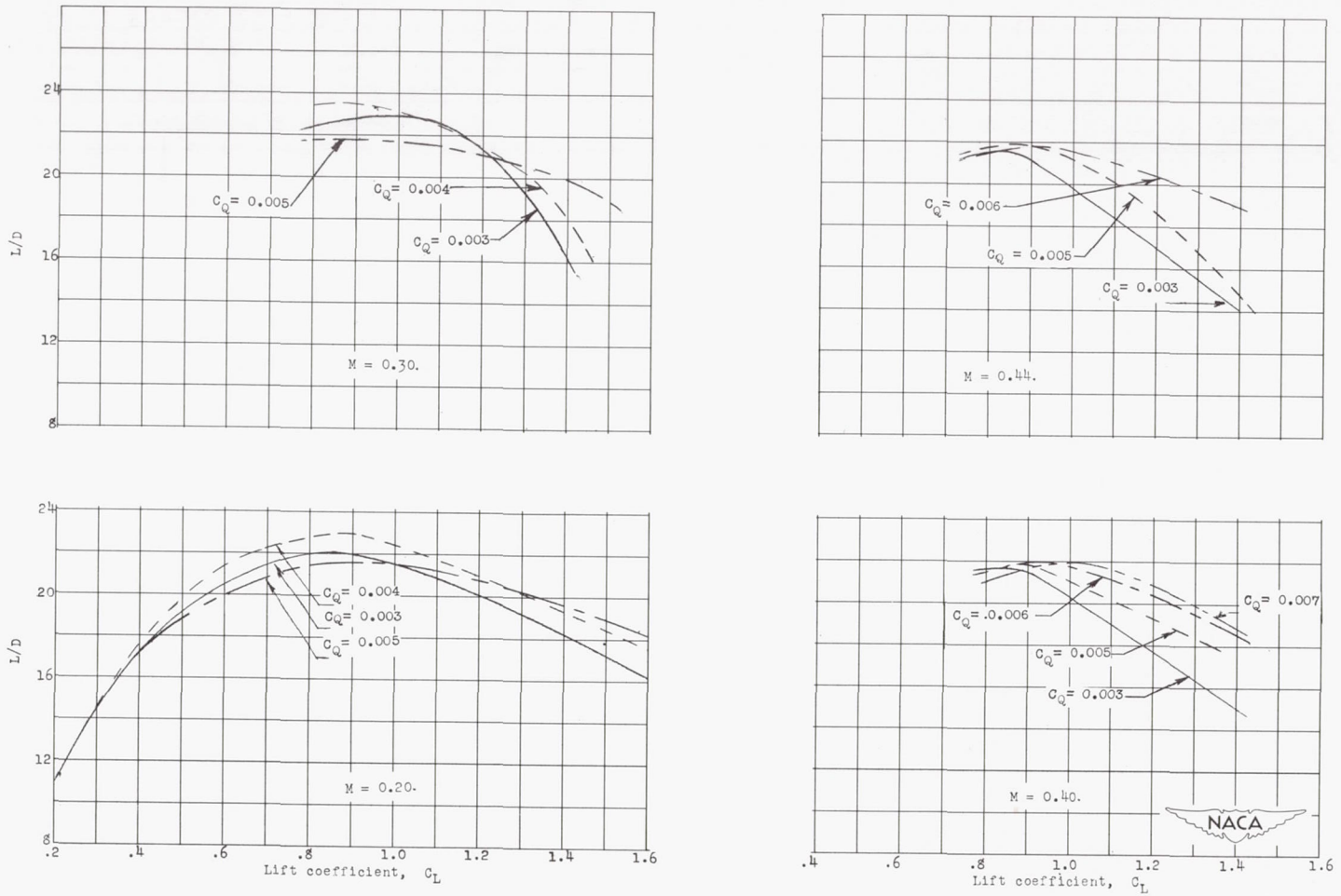
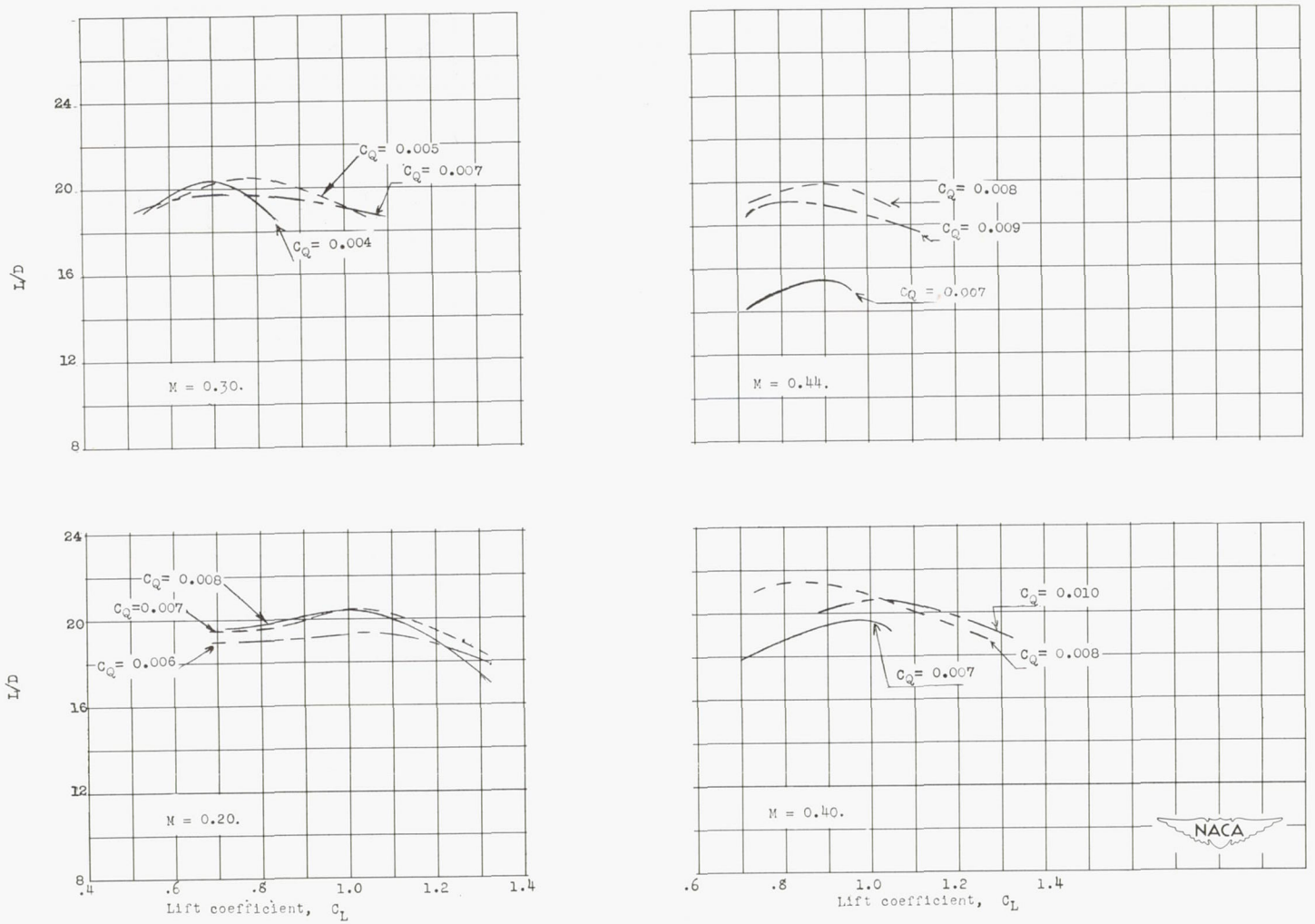


Figure 28.- Variation of pressure-loss coefficient with lift coefficient. Model II.



(a) Smooth wing.

Figure 29.- Variation of lift-drag ratio for various flow coefficients with Mach number. Model II.



(b) Roughness strips.

Figure 29.- Concluded.

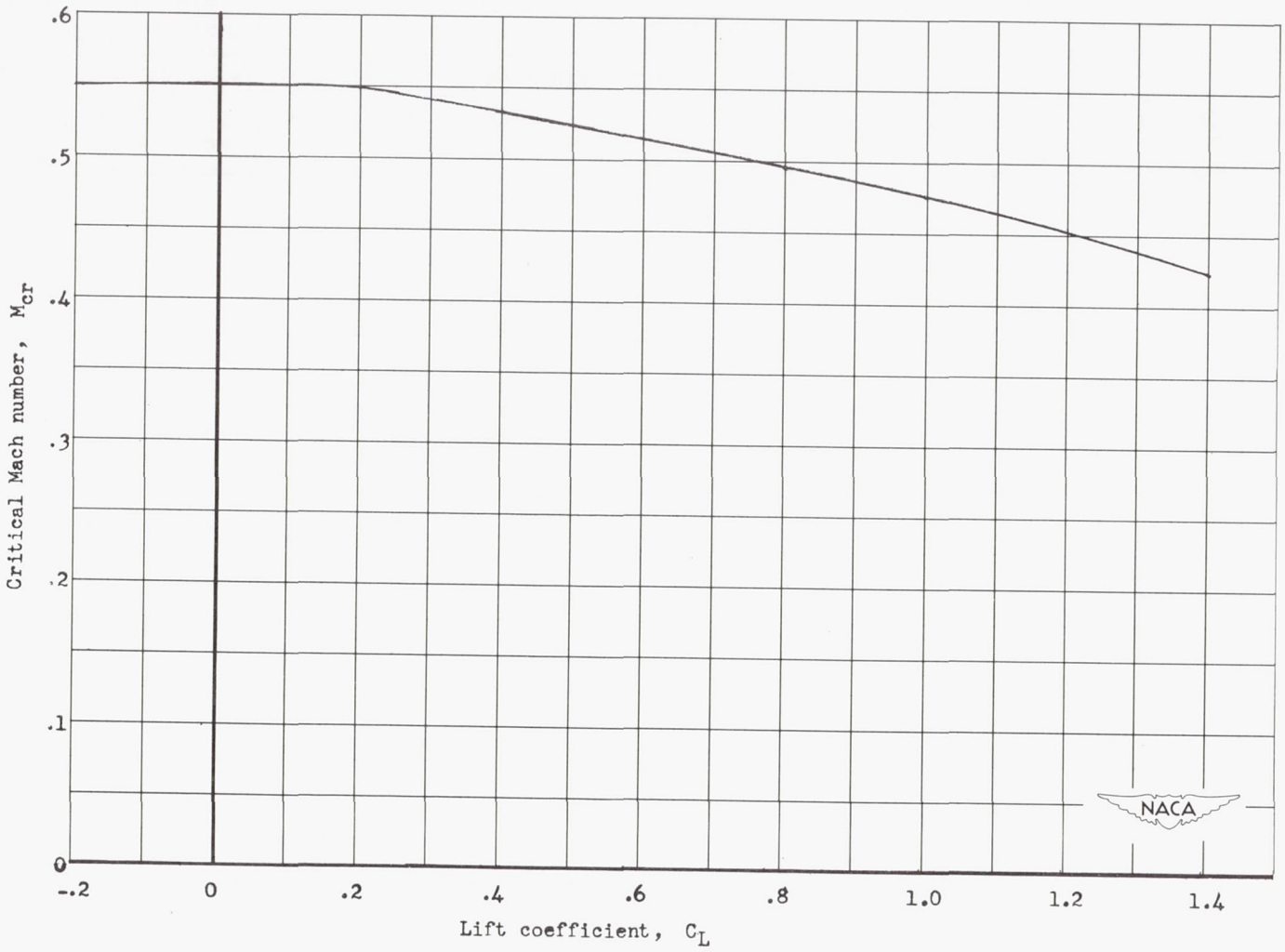


Figure 30.- Critical Mach numbers calculated by the method of reference 5 from low-speed pressure distributions obtained at the NACA 64,2-436 station on model I.

NACA-Langley - 8-5-53 - 1000